NATIONAL ADVISORY COMMITTEE FOR AERONAUTICS

TECHNICAL NOTE 3580

STALL PROPAGATION IN AXIAL-FLOW COMPRESSORS

By Alan H. Stenning, Anthony R. Kriebel,
and Stephen R. Montgomery

Massachusetts Institute of Technology

Washington
June 1956

NATIONAL ADVISORY COMMITTEE FOR AERONAUTICS

TECHNICAL NOTE 3580

STALL PROPAGATION IN AXIAL-FLOW COMPRESSORS

By Alan H. Stenning, Anthony R. Kriebel,
and Stephen R. Montgomery

SUMMARY

A theory of stall propagation in a cascade of airfoils of high solidity has been developed which includes the effects of finite blade chord and of the boundary-layer response to changes in angle of attack. The theory, based on the assumption that the flow behind the cascade consists of free jets discharging into a constant pressure region, is valid for small perturbations in velocity about a mean flow condition with finite pressure rise across the cascade, provided that the pressure fluctuations downstream of the cascade are much smaller than those upstream of the cascade. The solution for the velocity of stall propagation indicates that the velocity increases with the wave length of the stall cell, tending towards a limiting value for very large stall cells. The wave length of the stall cells at the beginning of rotating stall is dependent on the amount of time required for movement of the separation point on the airfoil (boundary-layer time delay).

For a stationary circular cascade and a single-stage axial-flow compressor, which were tested as part of this investigation, the theory predicts propagation velocities within 25 percent over a wide range of wave lengths. The experiments have confirmed that an increase in wave length is accompanied by an increase in propagation velocity, if other parameters are unchanged.

INTRODUCTION

In 1941, an investigation of diffusers for centrifugal compressors was made by Whittle's group, who were at that time developing the first British jet engine. They constructed a low-speed research rig with an observation window to study, with tufts of thread, the flow pattern at the diffuser entrance. For one type of diffuser the observation was made that at low mass flow rates a region of flow reversal traveled around the diffuser in the direction of wheel rotation, causing flow separation on each diffuser blade in turn. The velocity of the traveling stall was approximately one-sixth of the rotor tip speed. This was the first recorded example of the phenomenon now known as "rotating stall"

(ref. 1). The phenomenon apparently attracted little attention at the time and no further reference to it can be found, although in the light of recent discoveries it is possible that rotating stall was the cause of some blading failures in the early Whittle engines.

Several years later, at a time when compressor blade failures had become one of the major problems in the development of the axial-flow turbojet engine, rotating stall was rediscovered. Although the phenomenon was noted independently by several researchers, the first detailed study was apparently made by a research group working under the direction of Emmons (ref. 2). Using hot-wire techniques to investigate flow conditions in an axial compressor, Emmons' group found that, when the compressor was throttled, regions of low velocity appeared, traveling around the annulus in the direction of wheel rotation but at a lower speed. It was then apparent that blade failures previously unexplained were probably caused by vibratory stresses induced by rotating stall.

Later investigations of rotating stall in single-stage and multistage compressors are described in references 3 and 4.

The origin of rotating stall may readily be explained from consideration of the flow changes associated with blade stall. When a cascade of airfoils operates close to the stalled condition, a local increase in angle of attack on one airfoil may initiate stall on that blade. Because of the increased blockage effect of the separation region, some fluid spills around the affected channel, increasing the angle of attack on the blade above the stalled airfoil and decreasing the angle of attack on the blade below, so that the stalled region propagates along the blade row as shown in figure 1.

The main concern of the compressor designer is the frequency with which stalled regions pass the compressor blades. It is desirable to be able to predict this frequency for a given compressor and, if necessary, to alter it to avoid blade resonance. Investigations of rotating stall in axial compressors have yielded a bewildering variety of results, with no apparent order, so that at present the desired goal is not in sight. Some success has been attained in predicting the velocity of propagation of the stalled regions, but no means has been found of predicting the number of stalled regions present in a given compressor, and this number must be known before the exciting frequency can be calculated.

The investigation described in this report was undertaken in the belief that a thorough study of stall propagation in the simplest possible case (the single, two-dimensional cascade) was essential before approaching the more practical, but many times more complicated, problem of rotating stall in the axial compressor. Previous analyses of stall propagation in single cascades considered only disturbances of large

wave length and were unable to give any clues to the reasons for the appearance of stalled regions of varying wave lengths as the inlet angle to the blade row was changed. An analysis which included the effects of finite blade chord was therefore carried out and was accompanied by experimental work on a single cascade and on a single-stage compressor to determine the validity of the available theories and the effects which must be included in a successful theory.

This investigation has been conducted at the Massachusetts Institute of Technology under the sponsorship and with the financial assistance of the National Advisory Committee for Aeronautics. This report summarizes the results of an investigation in which many members of the Gas Turbine Laboratory staff have participated.

Mr. A. R. Kriebel designed the test cascade and was responsible for the success of the high-speed schlieren photography. Mr. S. R. Montgomery and Lieutenant J. J. Braun, USN, investigated the stall characteristics of the single-stage compressor and provided the data on stall propagation in the rotor. The original idea of using a circular cascade came from Professor E. S. Taylor, who has guided the project since its initiation. Professor Harold E. Edgerton gave generously of his time and lent much equipment.

SYMBOLS

A	area
$a_n(t)$, $b_n(t)$, $c_n(t)$, $d_n(t)$	functions of time
B	left-hand side of equation (19)
b	half wave length of disturbance
C	defined by equation (20)
C_{max}	value of C when $\frac{dC}{db} = 0$
C_p	cascade pressure coefficient, $\frac{p_2 - p_1}{(\rho/2)c_1^2}$
c	velocity
c_x	steady-state velocity in x-direction

c_y	steady-state velocity in y-direction
c_r	steady-state radial velocity
c_θ	steady-state tangential velocity
D	operator, $\frac{\partial}{\partial t}$
d	distance
F	function of β_1
f	frequency
G	functions defined by equations (11) and (12)
L	equivalent chord length of blade
M	Mach number
m	mass flow rate
N	number of symmetric stall cells
n	number of harmonic
p	stream pressure
p_o	total pressure
R	outside radius of guide-vane row
Re	Reynolds number
r,θ	polar coordinates
r_1	inside radius of cascade
r_2	outside radius of cascade
T	stream temperature
T_o	total temperature
t	time
u	total velocity in x- (or r-) direction

u' perturbation velocity in x- (or r-) direction

V velocity of stall propagation relative to blade row

V_n velocity of stall propagation of nth harmonic relative to blade row

v total velocity in y- (or θ-) direction

v' perturbation velocity in y- (or θ-) direction

x,y rectilinear coordinates

α discharge coefficient of cascade, $\frac{\text{Actual mass flow}}{\text{Ideal mass flow for same } (p_{o_1} - p_2)}$

$\alpha' = \frac{d\alpha}{d\ (\cot \beta_1)}$

β_1 inlet angle to cascade

β_2 outlet angle from cascade

λ_n nth root of characteristic equation

$\pi_m = \frac{\text{Wind-tunnel compressor tip speed}}{\text{Speed of sound in air entering compressor}}$

ρ density

σ cascade solidity, $\frac{\text{Chord}}{\text{Pitch}}$

τ time constant of boundary-layer delay

Φ total velocity potential

φ perturbation velocity potential

ω_n radian frequency of nth harmonic

Subscripts:

r partial derivative with respect to r

t partial derivative with respect to t

x partial derivative with respect to x

y	partial derivative with respect to y
θ	partial derivative with respect to θ

THEORY OF ROTATING STALL

Background

Theoretical investigations of rotating stall have previously been undertaken by Emmons, Sears, and Marble. In each case, the equations of motion were linearized, so that the analyses are strictly valid only for small perturbations in velocity about a mean flow condition. In any analysis of stall propagation, the results obtained depend on the assumptions made about (a) the nature of the flow field downstream of the cascade, (b) the form of the cascade characteristic, and (c) the relative importance of the different dynamic effects which govern the velocity of propagation of disturbances along the cascade. The possible assumptions which can be made will be discussed before reviewing the three theories.

The flow field immediately behind a stalled cascade in steady flow consists of streams of fluid, which have suffered little loss in stagnation pressure, separated by regions of low stagnation pressure as shown in figure 2. Downstream, mixing occurs between the high and low velocity regions, and at a distance of 10 chords or so from the cascade the velocity is approximately uniform across the wake. In analyzing stall propagation, some approximation to the real conditions in the unsteady flow behind the cascade must be made. Emphasis may be placed on the flow field immediately behind the cascade by considering the flow to consist of a number of free jets entering a region of constant pressure. Alternatively, the region where mixing is complete may be considered to be of greater importance and the velocity distribution downstream may be assumed continuous throughout the field. The true condition lies between these two extremes and may be closer to one or the other of them depending on the size of the propagating stall regions relative to the blade chord. If the disturbance is very large relative to the blade chord, then its effect will be felt far downstream and well beyond the mixing region. For this case, the mixing region can be neglected and the downstream flow field considered as a continuum. On the other hand, if the disturbance affects only two or three blades, it may be damped out within the mixing region and the downstream pressure changes will be small. The assumption of free jets discharging into a constant pressure chamber is then to be preferred.

The cascade performance may be represented by curves of pressure coefficient, circulation, or effective discharge coefficient as a function of inlet angle to the cascade. This function may be continuous or

discontinuous, and considerable disagreement exists as to which representation is the more accurate. This question will probably be settled only when dynamic measurements of cascade performance can be made.

In the most general case, three factors influence the speed of propagation of a disturbance along a cascade of airfoils in the stalled condition. These are (a) the time required for movement of the separation point on the airfoil after a change in inlet angle, which will be called the boundary-layer time delay, (b) the inertia of the fluid between the blades, and (c) the inertia of the fluid outside the cascade. The relative importance of these effects depends on the size of the stall region with respect to the blade chord, because the boundary-layer time delay and the inertia of the fluid within the blades are proportional to the blade chord, while the inertia of the fluid affected by the disturbance outside the cascade is proportional to the wave length of the disturbance. In consequence, when disturbances covering many blades are considered, the boundary-layer time delay and the inertia of the fluid within the cascade can be neglected.

The first analytical treatment of the problem was made by Emmons in 1951. He showed that the cascade could be represented as a series of channels in parallel, with variable-area outlets to represent the blockage effect of the separation regions. By investigating the stability of small disturbances ahead of the cascade, Emmons showed that, if a critical value of the derivative of the effective outlet area with respect to the angle of attack were obtained, disturbances would propagate unchanged along the cascade. For lower values of the derivative disturbances died out, while for higher values they were amplified. The propagation velocity was governed by an arbitrarily assumed time delay between changes in angle of attack and changes in the flow field ahead of the cascade. Pressure variations behind the cascade were assumed negligible and the cascade characteristic was assumed to be a continuous function of inlet angle. Emmons did not solve the dynamic equations of motion and, therefore, was unable to predict the velocity of propagation.

Sears, in 1953 (ref. 5), considered the case of disturbances which were large with respect to the blade chord and obtained the first complete solution. He assumed the existence of stalled regions moving with steady velocity along the cascade and calculated their velocity and the conditions required to produce them. The velocity field downstream of the cascade was considered to be continuous. Sears failed, however, to realize the full consequences of the assumption of large stall cells and introduced a boundary-layer phase lag which he believed to be of prime importance in influencing stall propagation. Although he obtained a solution showing stall propagation occurring with zero boundary-layer phase lag, in his conclusions Sears still stated that the speed of propagation of this phenomenon is determined by viscous effects. The

cascade characteristic was represented as a continuous function of inlet angle, and the mean flow condition was considered to be one in which there was no pressure rise across the cascade and no turning of the flow. The latter assumption is not a good one because rotating stall commences in a cascade at an angle of attack only slightly greater than that corresponding to the peak of the pressure-coefficient curve.

Marble, in 1954 (ref. 6), noted the inconsistency in Sears' analysis with regard to the boundary-layer delay and presented a theory for large stall cells in which the inertia of the fluid outside the blade row was considered to be of much greater importance than either the boundary-layer time delay or the inertia of the fluid between the blades. In addition, by a very ingenious method, he was able to treat the effect of a discontinuity in the cascade pressure-rise characteristic and show how the shape of the propagating wave changed as the mean inlet angle to the cascade increased. The propagation velocities obtained were the same as those predicted by Sears for zero boundary-layer phase lag. Marble's theory, like Sears', is valid only for a mean flow condition in which there is a very small pressure rise across the cascade, since a finite step in pressure is accompanied by finite velocity changes and the theory is based on the assumption of small perturbations in velocity.

In summation, the theories presented by Sears and Marble should predict the velocity (Sears-Marble value) of propagation of stalled regions along a cascade in cases where the stalled regions are so large that the effects of the boundary-layer delay, the inertia of the fluid within the blades, and the mixing region after the cascade can be neglected. They give no clues to the reasons for the appearance of different numbers of stall cells in a compressor as the compressor is throttled, and they are valid only if the cascade pressure coefficient is small when rotating stall commences.

In 1954, Stenning (ref. 7) presented a theory which treated the case where the inertia of the fluid within the cascade could not be neglected, allowing also a finite pressure rise across the cascade when rotating stall commenced. A later development of the theory includes the boundary-layer delay and offers a possible explanation of the varying number of stall cells which appear when a compressor is throttled. The complete analysis is presented in the following section.

Analysis of Stall Propagation in a Cascade

The main objective of the analysis is a consideration of stall propagation when the boundary-layer time delay and the inertia of the fluid within the cascade are considered as well as the free-stream inertia. As has already been suggested, for this case (which is one frequently encountered in practice), the pressure fluctuations downstream

of the cascade should be small compared with the upstream fluctuations, so that the assumption that the flow behind the cascade consists of free jets discharging into a constant pressure region appears to be the more accurate one.

The model representation of the cascade and the method of attack employed are similar to those used by Emmons. The advantage of this method is that it uses the classic techniques of stability analysis to determine whether disturbances will be amplified or will die away and thus gives a good physical understanding of the phenomenon.

Representation of cascade.- The analysis is based on the model shown in figure 3, with the cascade simulated by a series of channels of length L arranged in parallel and having variable-area outlets. The fluid enters the cascade at (1) with entrance angle β_1, is turned to flow angle β_2 at (3) in a short distance, and leaves the channel at (2). The assumption is made that the effect of stall produces a discrete region of flow separation, so that the wake behind the cascade consists of a number of free jets discharging into a region of constant pressure.

The ratio of exit area to inlet area A_2/A_3 is defined to be a function of β_1 as

$$\frac{A_2}{A_3} = \alpha = F\left(\cot \beta_1\right)$$

The assumption is made that local changes in α lag behind local changes in β_1 exponentially as shown in figure 4, so that for step changes in β_1

$$\delta\alpha = (\delta\alpha)_{ss}\left(1 - e^{-t/\tau}\right)$$

where $(\delta\alpha)_{ss}$ is the steady-state change in α corresponding to the change in β_1 and τ is the time constant of the boundary-layer time delay. Thus, in general, when β_1 changes continually

$$\tau \frac{\partial}{\partial t}(\delta\alpha) = (\delta\alpha)_{ss} - \delta\alpha$$

at any instant where $(\delta\alpha)_{ss}$ is the steady-state value of $\delta\alpha$, corresponding to the value of β_1 at that instant or $\delta\alpha = \frac{(\delta\alpha)_{ss}}{\tau D + 1}$ using operational notation where D denotes $\frac{\partial}{\partial t}$.

This representation of the boundary-layer response is an extreme oversimplification of a complex phenomenon which is not yet fully understood. It is, of course, not possible to consider the changes in effective exit area as independent of the fluid velocity in the passage since the fluid itself forms the "gate." However, the response assumed gives the simplest model which includes the boundary-layer delay and should at least yield some information on the effect of this delay.

The ratio A_2/A_3 is equivalent to the ratio

$$\frac{\text{Actual flow through cascade}}{\text{Ideal flow for same } (p_{o1} - p_2) \text{ with no losses}}$$

and is obtainable, for a real cascade, from test results.

It can be seen that $\alpha = A_2/A_3$ is a measure of the "swallowing capacity" of the cascade and must therefore be important when the possibility of flow spillage around the entrance is considered. For a real cascade, it can be shown that α is equivalent to

$$\frac{\cos \beta_1}{\cos \beta_2 \sqrt{1 - C_p}}$$

for a rectilinear cascade, where C_p is the pressure coefficient (see appendix A).

Additional assumptions are that the fluid is incompressible and frictionless and that changes in β_2 in the unsteady flow can be neglected. The blades are considered to be very close together, so that α may be taken as a continuous function of y.

For the initial analysis, the boundary-layer response is assumed fast compared with the inertia delays, so that τ is taken as zero. The effect of the boundary-layer delay is considered subsequently.

Solution in field before cascade.- The solution in the field before the cascade is obtained as follows:

The cascade lies on the y-axis in the xy plane. The fluid is considered to be incompressible. Perturbations are considered from a steady flow with inlet angle β_1 and velocity components c_x and c_y.

Since the flow entering the cascade is irrotational a velocity potential can be used. In the unsteady flow,

$$u = c_x + \varphi_x$$

$$v = c_y + \varphi_y$$

$$\Phi = c_x x + c_y y + \varphi$$

Where Φ is the total velocity potential and φ is the perturbation potential. From continuity, $\frac{\partial u}{\partial x} + \frac{\partial v}{\partial y} = 0$; that is, $\varphi_{xx} + \varphi_{yy} = 0$. Solutions to this equation are obtainable in the form

$$\varphi = \sum_{n=1}^{\infty} \left[\alpha_n(t) \cos \frac{n\pi y}{b} + b_n(t) \sin \frac{n\pi y}{b} \right] e^{\frac{n\pi x}{b}} \qquad (1)$$

representing periodic disturbances of half wave length b and satisfying the boundary condition, at $x = -\infty$,

$$\varphi_x = \varphi_y = 0$$

The stability of the disturbances depends on the time-dependent functions $a_n(t)$ and $b_n(t)$ which are as yet undetermined. From consideration of the dynamic equations, it is possible to find the conditions required for the disturbances to be damped, amplified, or propagated unchanged along the cascade.

From Euler's equation for unsteady flow,

$$\Phi_t + H = \text{Constant}$$

where

$$H = \frac{c^2}{2} + \frac{p}{\rho} = \frac{u^2 + v^2}{2} + \frac{p}{\rho}$$

For small perturbations from the steady flow,

$$\varphi_t + c\ \delta c + \frac{\delta p}{\rho} = 0 \qquad (2)$$

Equations (1) and (2) are valid in the region $-\infty < x < 0$.

Entry to cascade.- The equation for flow entering the cascade is derived as follows:

The distance (1) to (3) (fig. 3) is assumed small so that inertia effects between (1) and (3) may be neglected. Thus,

$$\frac{c_1^2}{2} + \frac{p_1}{\rho} = \frac{c_3^2}{2} + \frac{p_3}{\rho}$$

$$c_1\,\delta c_1 + \frac{\delta p_1}{\rho} = c_3\,\delta c_3 + \frac{\delta p_3}{\rho} \tag{3}$$

At (1), equation (2) may be rewritten

$$(\varphi_t)_1 + c_3 \delta c_3 + \frac{\delta p_3}{\rho} = 0 \tag{4}$$

Momentum effects in cascade.- In order to obtain the momentum effects in the cascade, the flow between (3) and (2) (fig. 3) is considered one-dimensional and the momentum equation in the l-direction is

$$\frac{\partial c}{\partial t} + c\,\frac{\partial c}{\partial l} + \frac{1}{\rho}\,\frac{\partial p}{\partial l} = 0$$

Integrating with respect to l from (3) to (2), with the assumptions that $c = c_3$ between (3) and (2) and that the change in velocity from c_3 to c_2 takes place in a short distance, gives

$$L\,\frac{\partial c_3}{\partial t} + \frac{c_2^2}{2} - \frac{c_3^2}{2} + \frac{p_2}{\rho} - \frac{p_3}{\rho} = 0$$

For small perturbations from a steady flow,

$$L\,\frac{\partial}{\partial t}(\delta c_3) + c_2\,\delta c_2 - c_3\,\delta c_3 - \frac{\delta p_3}{\rho} = 0 \tag{5}$$

if p_2 does not change. Eliminating $c_3\ \delta c_3 + \frac{\delta p_3}{\rho}$ between equations (4) and (5) gives

$$L\frac{\partial}{\partial t}(\delta c_3) + (\varphi_t)_1 + c_2\ \delta c_2 = 0 \tag{6}$$

From continuity,

$$A_3 c_3 = A_2 c_2$$

$$A_3\ \delta c_3 = A_2\ \delta c_2 + c_2\ \delta A_2$$

Thus,

$$\delta c_2 = \frac{A_3}{A_2}\ \delta c_3 - c_2\frac{\delta A_2}{A_2}$$

and

$$c_2\ \delta c_2 = \left(\frac{A_3}{A_2}\right)^2 c_3\ \delta c_3 - \left(\frac{A_3}{A_2}\right)^2 c_3^2\frac{\delta A_2}{A_2}$$

Also from continuity, $u = c_3 \cos\beta_2$ so that $\delta u = \varphi_x = \delta c_3 \cos\beta_2$. Substitution for c_3 and δc_3 yields

$$c_2\ \delta c_2 = \left(\frac{A_3}{A_2}\right)^2 \frac{c_x\varphi_x}{\cos^2\beta_2} - \left(\frac{A_3}{A_2}\right)^2 \frac{c_x^2}{\cos^2\beta_2}\frac{\delta A_2}{A_2}$$

By substituting this expression for $c_2\ \delta c_2$ in equation (6), the following equation is obtained at point (1):

$$\varphi_t + \frac{L}{\cos\beta_2}\varphi_{xt} + \frac{c_x\varphi_x}{a^2\cos^2\beta_2} - \frac{c_x^2}{a^2\cos^2\beta_2}\frac{\delta A_2}{A_2} = 0 \tag{7}$$

But,

$$\frac{\delta A_2}{A_2} = \frac{\delta\alpha}{\alpha}$$

$$= \frac{1}{\alpha}\frac{d\alpha}{d\,(\cot\beta_1)}\,\delta\,(\cot\beta_1)$$

$$= \frac{\alpha'}{\alpha}\,\delta(u/v)$$

$$= \frac{\alpha'}{\alpha}\,\frac{\varphi_x - \cot\beta_1\varphi_y}{c_y}$$

where

$$\alpha' = \frac{d\alpha}{d\,(\cot\beta_1)}$$

Thus, at ① (fig. 3),

$$\varphi_t + \frac{L}{\cos\beta_2}\varphi_{xt} + \frac{c_x\varphi_x}{\alpha^2\cos^2\beta_2}\left(1 - \frac{\cot\beta_1\alpha'}{\alpha}\right) + \frac{\cot^2\beta_1\alpha'}{\alpha^3\cos^2\beta_2}c_x\varphi_y = 0 \qquad (8)$$

This equation must be satisfied by φ at the entrance to the cascade, that is, at $x = 0$. By substituting the solution for φ (eq. (1)) into equation (8) and separating coefficients of $\cos\frac{n\pi y}{b}$ and $\sin\frac{n\pi y}{b}$, two simultaneous differential equations are obtained in terms of $a_n(t)$ and $b_n(t)$ as follows:

$$a_n\left[\left(\cos\beta_2 + \frac{Ln\pi}{b}\right)D + \frac{n\pi}{b}\frac{c_x}{\alpha^2\cos\beta_2}\left(1 - \frac{\cot\beta_1\alpha'}{\alpha}\right)\right] + b_n\left(\frac{n\pi}{b}\frac{\cot^2\beta_1\alpha' c_x}{\alpha^3\cos\beta_2}\right) = 0$$

$$b_n\left[\left(\cos\beta_2 + \frac{Ln\pi}{b}\right)D + \frac{n\pi}{b}\frac{c_x}{\alpha^2\cos\beta_2}\left(1 - \frac{\cot\beta_1\alpha'}{\alpha}\right)\right] - a_n\left(\frac{n\pi}{b}\frac{\cot^2\beta_1\alpha' c_x}{\alpha^3\cos\beta_2}\right) = 0$$

Assuming solutions of the form $a_n = A_n e^{\lambda_n t}$ and $b_n = B_n e^{\lambda_n t}$ gives the characteristic equation

$$\left[\left(\cos \beta_2 + \frac{Ln\pi}{b}\right)\lambda_n + \frac{n\pi}{b}\frac{c_x}{\alpha^2 \cos \beta_2}\left(1 - \frac{\cot \beta_1 \alpha'}{\alpha}\right)\right]^2 + \left(\frac{n\pi}{b}\frac{\cot^2 \beta_1 \alpha' c_x}{\alpha^3 \cos \beta_2}\right)^2 = 0 \tag{9}$$

The roots of this equation may represent oscillatory disturbances which are damped out, amplified, or persist unchanged depending on the value of the damping term containing $1 - \frac{\cot \beta_1 \alpha'}{\alpha}$. If $\alpha' < \frac{\alpha}{\cot \beta_1}$, the disturbance will die away. If $\alpha' > \frac{\alpha}{\cot \beta_1}$, it will be amplified beyond the range in which a linearized analysis is valid. If $\alpha' = \frac{\alpha}{\cot \beta_1}$ (fig. 5), the disturbance will persist and a_n and b_n will be of the form $A_n \cos \omega_n t + B_n \sin \omega_n t$ and $A_n \sin \omega_n t - B_n \cos \omega_n t$, respectively. The potential function then represents waves traveling along the cascade. At this point, the characteristic equation becomes

$$\lambda_n^2 + \left[\frac{\frac{n\pi}{b} \cot \beta_1 c_x}{\alpha^2 \cos \beta_2\left(\frac{Ln\pi}{b} + \cos \beta_2\right)}\right]^2 = 0$$

representing waves of frequency in radians per second

$$\omega_n = \frac{\frac{n\pi}{b} \cot \beta_1 c_x}{\alpha^2 \cos \beta_2\left(\frac{Ln\pi}{b} + \cos \beta_2\right)}$$

The velocity of wave propagation of the nth harmonic along the cascade V_n = (Frequency)(Wave length) or

$$V_n = \frac{\omega_n}{2\pi}\frac{2b}{n}$$

$$= \frac{\cot \beta_1 c_x}{\alpha^2 \cos \beta_2\left(\frac{Ln\pi}{b} + \cos \beta_2\right)}$$

$$\frac{V_n}{c_x} = \frac{\cot \beta_1}{\alpha^2 \cos \beta_2 \left(\frac{Ln\pi}{b} + \cos \beta_2 \right)}$$

This result indicates that the velocity of stall propagation increases with the size of the stall cell, the limiting value of V_n/c_x for stall cells covering many blades being $\frac{\cot \beta_1}{\alpha^2 \cos^2 \beta_2}$. In figures 6(a) and 6(b) $\alpha^2 V/c_x$ is plotted against β_1 for cascades with 10° and 15° turning angles and different values of $\pi L/b$. The velocity of propagation is taken as the velocity of the fundamental component of the wave. The expression for V_n/c_x includes the number of the harmonic n and indicates that higher harmonics travel more slowly than the primary wave. This is not in accord with experience and shows that a linearized analysis is inadequate in this respect.

The propagation velocity may be conveniently related to the cascade pressure rise (which is a more familiar parameter than α) by replacing α with its equivalent $\frac{\cos \beta_1}{\cos \beta_2 \sqrt{1 - C_p}}$. Then,

$$\frac{V_n}{c_x} = \frac{\cot \beta_1 (1 - C_p)}{\cos^2 \beta_1 \left(\frac{Ln\pi}{b \cos \beta_2} + 1 \right)}$$

$$\frac{V_n}{c_x} = \frac{2(1 - C_p)}{\sin 2\beta_1 \left(\frac{Ln\pi}{b \cos \beta_2} + 1 \right)}$$

For stall cells covering many blades, this expression reduces to

$$\frac{V}{c_x} = \frac{2(1 - C_p)}{\sin 2\beta_1}$$

It should be noted that, with the boundary-layer time delay neglected, no limitation is placed on the wave length of the disturbances. Consideration of the boundary-layer delay permits prediction of the size of the wave in addition to the velocity.

Interference effect of blade row upstream of cascade.- With the assumption that pressure changes downstream of the cascade may be neglected, it is not possible to treat the interference effect of an additional blade row behind the cascade. Upstream interference effects are, however, very easily determined. If a row of closely spaced blades of very large chord is situated a distance d from the cascade (fig. 7), then the perturbation velocity φ_x will be forced to zero at $x = -d$ because of the high inertia of the fluid within the guide vanes. In any practical case, φ_x will not be zero at $x = -d$ because of the finite chord of the guide vanes, but this approximation will permit an estimation of upstream interference. A solution for φ may then be found in the form

$$\varphi = \sum_{n=1}^{\infty} \left[a_n(t) \cos \frac{n\pi y}{b} + b_n(t) \sin \frac{n\pi y}{b} \right] \left[e^{\frac{n\pi x}{b}} + e^{\frac{-n\pi}{b}(x+2d)} \right]$$

satisfying the condition $\varphi_x = 0$ at $x = -d$. Substitution of this solution into equation (8) gives, for the case of undamped waves, when $\alpha' = \frac{\cot \beta_1}{\alpha}$,

$$\omega_n = \frac{\frac{n\pi}{b} \cot \beta_1 \, c_x}{\alpha^2 \cos \beta_2 \left[\frac{Ln\pi}{b} \frac{\left(1 - e^{\frac{-2n\pi d}{b}} \right)}{\left(1 + e^{\frac{-2n\pi d}{b}} \right)} + \cos \beta_2 \right]}$$

$$\frac{V_n}{c_x} = \frac{\cot \beta_1}{\alpha^2 \cos \beta_2 \left(\frac{Ln\pi}{b} \frac{1 - e^{\frac{-2n\pi d}{b}}}{1 + e^{\frac{-2n\pi d}{b}}} + \cos \beta_2 \right)}$$

The equivalent expression for propagation velocity in terms of the cascade pressure coefficient is

$$\frac{V_n}{c_x} = \frac{2\left(1 - C_p\right)}{\sin 2\beta_1 \left(\frac{Ln\pi}{b} \frac{1 - e^{\frac{-2n\pi d}{b}}}{1 + e^{\frac{-2n\pi d}{b}}} + 1 \right)}$$

Thus, interference increases the velocity of propagation for $Ln\pi/b$ of order unity but does not change it for disturbances with wave lengths which are large compared with the blade chord. If d/b is very small, then the coefficient of $Ln\pi/b$ is effectively zero and $\frac{V_n}{c_x} = \frac{\cot \beta_1}{\alpha^2 \cos^2 \beta_2}$, which is the same result as that obtained without upstream interference when the wave length is large. The addition of a row of guide vanes upstream of the cascade therefore decreases the influence of the inertia of the fluid within the stalled cascade on the velocity of propagation.

An approximation to the velocity of stall propagation relative to the rotor in a single-stage compressor with guide vanes close to the wheel thus may be obtained by putting $\frac{V_n}{c_x} = \frac{\cot \beta_1}{\alpha^2 \cos^2 \beta_2}$. This should be valid only when the blades are stalled from root to tip so that the flow is effectively two-dimensional.

Effects of boundary-layer delay.- The time constant τ of the boundary-layer delay will now be included in the analysis to determine the additional limitations it imposes on stall propagation. If $\delta\alpha = \frac{\alpha'}{\tau D + 1} \delta (\cot \beta_1)$ is substituted into equation (7), the equation satisfied by φ at (1) is

$$\tau\varphi_{tt} + \frac{L\tau}{\cos \beta_2} \varphi_{xtt} + \varphi_t + \varphi_{xt}\left(\frac{L}{\cos \beta_2} + \frac{\tau c_x}{\alpha^2 \cos^2 \beta_2}\right) + \frac{c_x \varphi_x}{\alpha^2 \cos^2 \beta_2}\left(1 - \frac{\cot \beta_1 \alpha'}{\alpha}\right) - \frac{\cot^2 \beta_1 \alpha'}{\alpha^3 \cos^2 \beta_2} c_x \varphi_y = 0 \tag{10}$$

Inserting the solution for φ (eq. (1)) and separating the coefficients of $\cos \frac{n\pi y}{b}$ and $\sin \frac{n\pi y}{b}$ give two second-order differential equations in terms of a_n and b_n. Taking solutions of the form $a_n = A_n e^{\lambda n t}$ and $b_n = B_n e^{\lambda n t}$ gives the following characteristic equation for λ_n:

$$\left\{\left(\tau + \frac{n\pi}{b}\frac{L\tau}{\cos\beta_2}\right)\lambda_n^2 + \left[1 + \frac{n\pi}{b}\left(\frac{L}{\cos\beta_2} + \frac{\tau c_x}{\alpha^2\cos^2\beta_2}\right)\right]\lambda_n + \frac{n\pi}{b}\frac{c_x}{\alpha^2\cos^2\beta_2}\left(1 - \frac{\cot\beta_1\alpha'}{\alpha}\right)\right\}^2 + \left(\frac{n\pi}{b}\frac{\cot^2\beta_1\alpha' c_x}{\alpha^3\cos^2\beta_2}\right)^2 = 0 \tag{11}$$

This equation will be examined to find the conditions for undamped oscillations in time. Equation (11) is of the form

$$\left(G_1\lambda_n^2 + G_2\lambda_n + G_3\right)^2 + G_4^2 = 0 \tag{12}$$

For undamped oscillations, $\lambda_n = \pm i\omega_n$ must be a root. With $\lambda_n = i\omega_n$ a solution is obtained as follows:

$$\left(-G_1\omega_n^2 + iG_2\omega_n + G_3\right)^2 + G_4^2 = 0 \tag{13}$$

With $\lambda_n = -i\omega_n$ a solution is obtained as follows:

$$\left(-G_1\omega_n^2 - iG_2\omega_n + G_3\right)^2 + G_4^2 = 0 \tag{14}$$

Subtracting equation (14) from equation (13) and factoring give

$$2\left(-G_1\omega_n^2 + G_3\right)\left(2iG_2\omega_n\right) = 0$$

Thus, if $\lambda_n = \pm i\omega_n$ is a root of equation (12), then $\omega_n^2 = G_3/G_1$. Putting $\omega_n = \sqrt{G_3/G_1}$ in equation (13) gives

$$\left(-G_3 + iG_2\sqrt{G_3/G_1} + G_3\right)^2 + G_4^2 = 0$$

$$-G_2^2\left(G_3/G_1\right) + G_4^2 = 0$$

or

$$G_3/G_1 = \left(G_4/G_2\right)^2 \tag{15}$$

The requirements for an undamped oscillatory solution to equation (12) are, therefore, that $G_3/G_1 = \left(G_4/G_2\right)^2$. With this requirement satisfied, two of the roots of the equation are $\pm i\omega_n$ where $\omega_n = G_4/G_2$. A factor of the equation is then $\lambda_n^2 + \left(G_4/G_2\right)^2$ and the remaining two roots satisfy the equation

$$\lambda_n^2 + 2\left(G_2/G_1\right)\lambda_n + \left[\left(G_4/G_2\right)^2 + \left(G_2/G_1\right)^2\right] = 0 \tag{16}$$

For the remaining two roots to be stable the coefficient of λ_n in equation (16) must be positive; that is, G_2/G_1 must be positive.

It can be seen, therefore, that for equation (12) to have roots representing undamped oscillations of frequency ω_n (1) all coefficients must be positive and (2) $G_3/G_1 = \left(G_4/G_2\right)^2$. Under these circumstances, $\omega_n = G_4/G_2$. Applying these results to equation (11), the requirement for stall propagation is

$$\frac{\frac{n\pi}{b}\frac{c_x}{\alpha^2\cos^2\beta_2}\left(1 - \frac{\cot\beta_1\alpha'}{\alpha}\right)}{\tau\left(1 + \frac{n\pi}{b}\frac{L}{\cos\beta_2}\right)} = \frac{\left(\frac{n\pi}{b}\frac{\cot^2\beta_1\alpha' c_x}{\alpha^3\cos^2\beta_2}\right)^2}{\left[1 + \frac{n\pi}{b}\left(\frac{L}{\cos\beta_2} + \frac{\tau c_x}{\alpha^2\cos^2\beta_2}\right)\right]^2} \tag{17}$$

and the frequency of the oscillations at any point in radians per second is

$$\omega_n = \frac{\frac{n\pi}{b}\frac{\cot^2\beta_1\alpha' c_x}{\alpha^3\cos^2\beta_2}}{1 + \frac{n\pi}{b}\left(\frac{L}{\cos\beta_2} + \frac{\tau c_x}{\alpha^2\cos^2\beta_2}\right)} \tag{18}$$

If $\tau = 0$ the same results are obtained as in the earlier analysis. The importance of this solution lies not in the precise relationship but in the fact that a relation is established among L/b, τ, α, α', β_1, and β_2 which makes stall propagation possible. More explicitly, since for a given cascade τ, α, α', and β_2 all depend on β_1, a relationship has been found between L/b and β_1 for stall propagation. Thus, over

a range of inlet angles, stall propagation can occur and the size of the stall cell will depend on the inlet angle. This result may explain the variation in size and number of stall cells found in an axial compressor stage over the working range of angle of attack.

It can be seen that, with the boundary-layer delay included in the analysis, stall propagation occurs with $\frac{\cot \beta_1 \alpha'}{\alpha}$ less than unity, so that the frequency of the disturbances is lower than the frequency of the stalls of the same wave length when the boundary layer is left out. The boundary-layer delay therefore has the effect of decreasing the velocities of propagation of the stalled regions. The boundary-layer time constant should be approximately of the order L/c_3, so that the boundary-layer delay may be as important as the inertia delay of the fluid within the cascade and will have little effect on the velocity of propagation of large stall cells.

Calculation of wave length when rotating stall commences.- It is now possible, without making any additional assumptions, to predict the wave length of the disturbances when rotating stall commences. Because of the simple representation employed for the boundary-layer response, it would be unwise to attempt to derive numerical values from this result, but it is of interest inasmuch as the main features of the phenomenon can be reproduced with a simple model.

When equation (17), which can be rewritten as

$$\frac{1 - \frac{\cot \beta_1 \alpha'}{\alpha}}{\frac{\tau \cot^4 \beta_1 (\alpha')^2 c_x}{\alpha^4 \cos^2 \beta_2}} = \frac{\frac{n\pi}{b}\left(1 + \frac{n\pi}{b} \frac{L}{\cos \beta_2}\right)}{\left[1 + \frac{n\pi}{b}\left(\frac{L}{\cos \beta_2} + \frac{\tau c_x}{\alpha^2 \cos^2 \beta_2}\right)\right]^2} \tag{19}$$

is satisfied, stall propagation is possible. It can be seen that, as the inlet angle β_1 to the cascade is increased and flow separation commences on the airfoils, α' will increase from almost zero to a positive quantity. The group on the left side of the equation (denoted by B) will therefore have a value which begins as a large positive quantity at the design point and decreases as β_1 is increased. At any setting of β_1, the group on the right side of the equation (denoted by C) can have an infinite number of values for each harmonic, depending on the value of b assumed. Considering only the primary component of the wave ($n = 1$), there will, however, be a maximum value of C corresponding to a wave length which might be considered as the wave length which is closest to being propagated. As β_1 is increased, the maximum possible

value of C can be computed for each value of β_1 and compared with the value of B (see fig. 8), which will, in general, be larger than the value of C. However, as β_1 is increased the difference between B and C shrinks until, at the critical value of β_1, the maximum value of C corresponds to the value of B at that point and stall propagation becomes possible for the wave length which yields this value of C. The problem is, therefore, the determination of the value of b which gives C_{max}.

For the primary component of the wave

$$C = \frac{\frac{\pi}{b}\left(1 + \frac{\pi}{b}\frac{L}{\cos\beta_2}\right)}{\left[1 + \frac{\pi}{b}\left(\frac{L}{\cos\beta_2} + \frac{\tau c_x}{\alpha^2\cos^2\beta_2}\right)\right]^2}$$

$$= \frac{\pi\left(b + \frac{\pi L}{\cos\beta_2}\right)}{\left[b + \pi\left(\frac{L}{\cos\beta_2} + \frac{\tau c_x}{\alpha^2\cos^2\beta_2}\right)\right]^2} \qquad (20)$$

For a maximum (or minimum) value of C, $dC/db = 0$ and this occurs when

$$b = \frac{\pi L}{\cos\beta_2}\left[\frac{\tau}{\alpha^2(L/c_3)} - 1\right]$$

A study of the expression for C shows that this value of b gives a maximum value of C, at a value of b which may be positive or negative depending on whether $\frac{\tau}{\alpha^2(L/c_3)}$ is greater than, or less than, unity.

There are now two possibilities. If $\frac{\tau}{\alpha^2(L/c_3)} > 1$, then, for positive (i.e., real) values of b, C has a maximum value when $b = \frac{\pi L}{\cos\beta_2}\left[\frac{\tau}{\alpha^2(L/c_3)} - 1\right]$ and this will be the value of b when stall propagation commences. If $\frac{\tau}{\alpha^2(L/c_3)} < 1$, then the maximum value of C for positive values of b occurs when $b = 0$, and stall propagation will commence with the smallest values of b that are physically possible.

Thus, the wave length is governed by the ratio $\frac{\tau}{(L/c_3)}$ which is the ratio of the boundary-layer time delay to the inertia delay of the fluid within the cascade.

Stall propagation in circular, radial-flow cascade.- For a radial-outflow cascade of the type used for the experimental study (fig. 9), an expression for propagation velocity may be derived in $r\theta$ coordinates (see appendix B).

With guide-vane interference effects included, but omitting the boundary-layer time delay,

$$\frac{V}{c_{r_1}} = \left(\frac{r_1}{r_2}\right)^2 \frac{\cot \beta_1}{\alpha^2 \cos \beta_2 \left[\frac{LN}{r_1} \frac{1 - (R/r_1)^{2N}}{1 + (R/r_1)^{2N}} + \cos \beta_2\right]}$$

where r_1/r_2 is the ratio $\frac{\text{Inside radius of cascade}}{\text{Outside radius of cascade}}$, R is the outside radius of the guide-vane row, and N is the number of stall cells in the cascade. Consideration of the boundary-layer time delay yields lower values of V/c_{r_1} than does the expression given above.

In terms of the cascade pressure coefficient

$$\frac{V}{c_{r_1}} = \frac{2\left(1 - c_p\right)}{\sin 2\beta_1 \left[\frac{LN}{r_1 \cos \beta_2} \frac{1 - (R/r_1)^{2N}}{1 + (R/r_1)^{2N}} + 1\right]}$$

and this reduces to the same form as that for the rectangular cascade when the stall cells are very large or the gap between the guide vanes and the cascade is small.

Discussion of Solutions

The most important point of difference between the present analysis and the analyses of Sears and Marble is the assumption made here that downstream pressure fluctuations may be neglected. For the case considered by Sears (that with no pressure rise across the cascade when stall propagation occurs), $C_p = 0$ and the present analysis then yields,

for disturbances with large wave length, $\frac{V}{c_x} = \frac{2}{\sin 2\beta_1}$. This is double the value obtained by Sears. Because C_p always lies in the range 0.3 to 0.6 when stall propagation commences, the values for propagation velocity given by the present theory are never double Sears' predicted values in any practical case, but may be greater or less than these depending on the pressure rise and whether the wave length of the disturbance is large with respect to the blade chord or of the same order of magnitude.

The values of propagation velocity predicted when the boundary-layer delay is neglected should be larger than those obtained experimentally, with the difference most pronounced for the case of disturbances covering only a few airfoils when the boundary-layer delay will have an important effect. An increase in the wave length of the stall cells should be accompanied by an increase in propagation velocity, if other variables are unchanged.

EXPERIMENTAL INVESTIGATION OF ROTATING STALL

Experimental work has been carried out using both a stationary cascade and a single-stage axial-flow compressor. This combination has proved exceedingly useful because a wide range of stall wave lengths could be examined and the measured characteristics compared with theory. In addition, a comparison of phenomena observed in the two test rigs has given an indication of the value and limitations of the circular cascade as a research tool to reproduce effects found in turbomachines.

Stationary Cascade

Apparatus and procedure.- In order to obtain the simplest possible type of flow in which a stable rotating-stall pattern could be observed, the cascade was constructed in the form of a circle between two flat plates (fig. 10). Air flows outward through the cascade, and the angle of incidence of the air entering the blades is controlled by a set of variable-angle nozzles ahead of the cascade (fig. 11). There are 54 compressor blades and an equal number of nozzles. Provision has been made for removal of the wall boundary layers by suction through slots machined in the casing (fig. 12). Air enters the test section through two pipes parallel with the central axis of the cascade and turns into the plane of the cascade before being accelerated in the nozzles. After leaving the cascade, the air is collected in a scroll and returned to the compressors.

An exterior view of the stationary circular cascade tunnel is shown in figure 13 and the longitudinal section and end elevation are depicted schematically in figure 14. The test section of the cascade tunnel is shown in figure 15. A schematic diagram of the flow circuit with the state conditions of the fluid tabulated for a typical operating condition is given in figure 16. With the closed-circuit arrangement, the Reynolds number and Mach number may be varied independently by changing the pressure level in the circuit. Reynolds numbers up to 300,000 (based on blade chord and conditions entering the cascade) and approach Mach numbers up to 0.8 are attainable.

The dimensions of the span and chord of the compressor cascade blading are 1.71 inches and 0.96 inch, respectively (fig. 12), and the airfoil section is shown in figure 11. The airfoil shape was obtained by conformal mapping of a rectilinear cascade into a circular cascade with radius ratio r_1/r_2 of 1.09. In the transformed cascade, the chord of the airfoil (defined as the straight line joining the centers of curvature of the leading and trailing edges) makes an angle of 42° with the radius through the leading edge (fig. 11.) The design-point inlet air angle of 48.5° measured from the radius and the outlet air angle is 38°. The blades of the cascade are located in position by pins which fit into holes drilled in the casing on a circle of radius 8.23 inches (figs. 10 and 12). After the stagger angle has been set, the blades are clamped into position at one end with bar clamps which fit over the ends of the pins and fasten adjacent blades together in pairs. It is thus possible to change the stagger angle of the cascade by loosening the clamps and resetting the blades. A different procedure is required for the three blades in the observation window since clamps would obscure the picture. These blades are retained in position by a wire soldered to their trailing edges and to the trailing edges of the clamped blades adjacent to the window.

At the commencement of the test program, difficulty was encountered with frequent torsion failures of the pins on the clamped ends of the blades. In addition, blade vibration caused chipping of the optical flats around the pins (showing as a circular blemish on the schlieren photographs) and the solder failed to hold the connecting wire to the blades in the window. These problems were ameliorated, though not completely solved, by cementing the blades to the casing on the clamped side and covering the pins of the blades in the test window with cement before inserting them in the window, thus increasing the damping and also cushioning the surface of the glass.

The design of the test rig and cascade is described in detail in references 8 and 9.

Instrumentation.- The observations made in the cascade may be divided into two classes, measurements of mean or steady-state values of

pressure, velocity, and flow direction and observations of instantaneous values of these parameters and of the changes in the flow field around the airfoils in rotating stall.

To obtain mean values of static pressures before and after the cascade, three pressure taps were fitted before the cascade at 120° from each other on a circle of 7.69-inch radius, and three pressure taps were mounted behind the cascade between the first three on a circle of 8.94-inch radius (fig. 12). Total-pressure probes were mounted in both inlet pipes to permit a total-pressure traverse before the nozzles, and the test window could be removed and replaced by a small traversing gear to obtain a total-pressure traverse ahead of the blades in the window.

The air angle leaving the cascade was measured with an uncertainty of ±2° using tufts attached to the connecting wire. The air angle entering the cascade was assumed equal to the nozzle outlet angle, since flow deviation is small for nozzles and the nozzles were so close together that accurate measurement of the air angle could not be obtained. An error of the order ±2° is therefore possible in the air inlet angle.

The mass flow through the cascade was obtained with an estimated accuracy of ±1/2 percent using a standard A.S.M.E. orifice meter. The total temperature leaving the compressor was measured using a thermocouple with an accuracy of ±2° F. From a knowledge of mass flow, air angle, total temperature, and static pressure, it was possible to compute the magnitude of the parameter $m\sqrt{T_o}/A_p$ entering the cascade from which, using gas tables for compressible flow, the mean entry Mach number, velocity, and total pressure could be found. A check on the accuracy of this method of calculating the conditions entering the cascade was available, inasmuch as the mean total pressure obtained should be very close to the average value found from a total-pressure traverse ahead of the cascade. A comparison of the two values at several operating points showed agreement within 0.5 percent, so that it was not necessary to make total-pressure traverses ahead of the cascade at each operating condition to find the mean total pressure.

For observations in the unsteady flow, the main instrument used was the Gas Turbine Laboratory portable schlieren apparatus, which proved effective for entry Mach numbers to the cascade as low as 0.2. Schlieren photographs were taken using a General Radio 35-millimeter high-speed camera, and a 16-millimeter Fastax camera, in conjunction with an Edgerton high-speed stroboscopic flash unit operated at flash rates up to 6,000 cps. The schlieren photographs showed the propagation velocity and the frequency of the rotating stalls, as well as the changes in air angle ahead of the cascade and the nature of the flow around the airfoils. A pair of hot-wire instruments gave another method of calculating the propagation velocity and number of stall cells and also showed qualitatively the nature of the velocity fluctuations. Pressure fluctuations before and after the cascade were compared by recording the signals from barium titanate crystals connected to static pressure taps.

Cascade performance.- before commencing the test program, total-pressure traverses were made in the inlet pipes and ahead of the blades in the test window. The thickness of the boundary layer in each inlet pipe was of the order of 0.1 inch and outside the boundary layer a maximum variation in total pressure equal to 8 percent of the mean dynamic pressure was observed, so that the total variation in velocity outside the boundary layer did not exceed 4 percent of the mean velocity. Variation in mean total pressure between the two inlet pipes did not exceed 3 percent of the mean dynamic pressure in the inlet pipes. In spite of the uniformity of the conditions entering the test section, considerable asymmetry in static pressure around the cascade was observed behind the nozzles, especially when the inlet angle β_1 to the cascade was low. At the design inlet angle, the total variation in static pressure around the cascade was 12 percent of the mean dynamic pressure leaving the nozzles. The asymmetry gradually disappeared as the rotating stall region was entered. These pressure variations were too large to be explainable by errors in nozzle-throat area. Also, the scroll shape should have had little upstream effect since the velocity in the scroll was very low. The most plausible explanation of the pressure variation around the cascade appears to lie in the possible presence of regions of separated flow within the duct which turned the flow leaving the inlet pipes into the plane of the cascade. Because of the space requirements of the schlieren apparatus, the duct was designed for no acceleration of the air as it turned, so that unfavorable pressure gradients in some areas may have caused flow separation before the nozzles. This effect would explain the decrease in the percentage asymmetry with increasing β_1, since upstream irregularities become less important as the pressure drop across the nozzles increases.

Ahead of the blades in the test window, variations in total pressure outside the wall boundary layers and the nozzle wakes were less than 5 percent of the mean dynamic pressure entering the cascade. The thickness of the wall boundary layers was of the order of 0.050 inch and the width of the nozzle wakes was approximately 0.070 inch.

The cascade performance was obtained in terms of the pressure rise across the cascade and in terms of the cascade outlet angle and is shown in figures 17 and 18 in which the cascade pressure coefficient C_p and the outlet angle β_2 measured from the radial direction are plotted versus β_1. It was found most convenient to operate the wind-tunnel compressors at constant rotational speed during a test run and to vary the air angle entering the cascade. Because of the compressor characteristic, this procedure resulted in almost constant mass flow through the cascade at any one rotational speed, independent of nozzle angle; and, in consequence, the Mach number leaving the nozzles increased as the nozzles were closed. Each curve in figure 17 corresponds to a constant value of the ratio $\frac{\text{Wind-tunnel compressor tip speed}}{\text{Speed of sound in air entering compressor}}$ denoted by π_m, and in figure 19 the Mach number entering the cascade is

plotted against β_1 for each of the three compressor speeds used. It can be seen in figure 17 that, for any value of β_1, there is a slight increase in C_p with increasing values of π_m. Within experimental error, no change in β_2 with Mach number could be determined.

Starting at an inlet angle of 42°, the pressure coefficient increases with β_1 until at 48° the curve flattens out briefly before rising again. The explanation of this dip lies in the fact that the nozzle wakes wash over the airfoils at a value of β_1 equal to 49° and have a serious effect on the cascade performance. The pressure coefficient then rises once more until a peak value is attained at an inlet angle of 56°. Thereafter, the pressure coefficient falls, until when β_1 equals 59° the curve starts to flatten, has a minimum value at 60°, a second peak at 63°, and then falls off again. The nozzle wakes cross the airfoils a second time when β_1 attains a value of 60° and at this point some unsteadiness was observed in the nozzle and cascade wakes, but stall propagation did not begin until the nozzle wakes passed the cascade. Random stalls were observed at an inlet angle of 61°, and periodic rotating stall commenced at an inlet angle of 64°.

It has been suggested that the temporary rise in pressure coefficient after initiation of the unsteady flow may be partly due to the increase in the root-mean-square value of the velocity entering the cascade. For a given inlet angle and mass flow rate in an unsteady flow, the mean pressure rise across the cascade is proportional to the time mean value of velocity squared, which increases as the velocity fluctuations become larger.

At the lowest compressor speed, the Mach number entering the cascade does not exceed 0.35, so that compressibility effects should be small and the experimental results may be used to test the theory presented previously. Using the method of appendix A, α has been calculated for each inlet angle up to the point where rotating stall commences and is plotted against $\cot \beta_1$ in figure 20. In the region before rotating stall begins, the curve is practically a straight line, with a gradient very close to the value predicted by the theory, the tangent passing slightly below the origin instead of through it. This result is in agreement with experimental evidence for rectilinear cascades presented by Emmons, Pearson, and Grant, in reference 2. In the circular cascade, rotating stall started at a value of α of approximately 0.80. It is, of course, impossible to find values of α for higher angles of attack in the rotating-stall region because of the unsteady flow, and the nozzle angle could not be increased sufficiently to pass through the unsteady flow region into a state of steady, fully stalled flow.

Schlieren photographs of the airfoils in the steady flow are presented in figure 21, at inlet angles of 42°, 46°, 49.5°, 53.2°, 56.8°, and 60.4°. The nozzle wakes and the cascade boundary layers are visible and the forward movement of the separation point with increasing β_1 can be observed.

Rotating stall in cascade.- As the nozzle angle was increased beyond 60°, the onset of rotating stall was accompanied by an increase in air noise from the apparatus, with a sharp intensification of the sound at 64° when full rotating stall commenced. For inlet Mach numbers above 0.5, lambda shocks appeared on the upper surface of the airfoils at high nozzle angles and the occurrence of these shock waves was signalled by a high-pitched screaming sound. The rotating-stall phenomena at low Mach numbers will be described first, since compressibility effects had a strong influence on the periodicity of the stall pattern.

To obtain satisfactory schlieren pictures, M_1 was required to be at least 0.2. In consequence, a compressor π_m of 0.173 (with M_1 ranging from 0.2 to 0.35) was most suitable for evaluation of rotating-stall phenomena at low Mach numbers and extensive testing was carried out at this speed setting of the wind-tunnel compressor. As can be seen from figure 21(f), just before the transition from steady flow to random stall occurred, the separation point on the suction surface of the airfoils was approximately 30 percent of the chord length rearward of the leading edge. A 1° increase in angle of attack from this point was sufficient to start random stall.

In this region of operation, the disturbance did not always propagate from blade to blade across the window but would frequently die out before reaching the last blade. Small differences in blade setting may have been responsible for this effect, since the possible variation from the nominal setting was estimated at ±1°. Figure 22(a) shows one cycle of stall and unstall in the random-stall regime. Some of the pictures taken in this region of operation showed the airfoils in the window remaining stalled for 20 to 30 milliseconds before unstalling, while others revealed stalls propagating across the window at intervals of 5 to 10 milliseconds. With increasing β_1, the disturbances appeared more regularly until at $\beta_1 = 64°$ the disturbances crossed the window at time intervals ranging from 3.2 to 5.6 milliseconds and could now be properly called rotating stall (fig. 22(b)). An airfoil was now stalled for approximately 40 percent of the time, and the wave length of the stalls was about six blade spacings. With further increases in β_1, the stalls appeared more regularly and at $\beta_1 = 67°$ (fig. 22(c)) the time intervals between disturbances varied only from 3.0 to 3.6 milliseconds. From the film records the velocity of propagation could be calculated within 5 percent and it was found that at any nozzle setting there was little variation in propagation velocity between stall cells but that the average propagation velocity increased from 90 fps to 120 fps

as β_1 was increased from 63° to 67°. Because of the variation in the time interval between stalls and the uncertainty in propagation velocity, the number of stall cells could be estimated only within about one cell, but there appeared to be approximately 9 cells in the cascade at $\beta_1 = 64°$, with the number increasing to 11 at $\beta_1 = 67°$. In table I, the measured propagation velocities are tabulated and compared with the results obtained using hot-wire equipment.

Over the whole range of inlet angles for which rotating stall was obtained, it was found that the time required to unstall an airfoil was always greater than the time required to stall an airfoil, the former process requiring approximately 0.6 to 0.8 millisecond, while the latter was completed in 0.4 to 0.5 millisecond (figs. 22 and 23). That this should be the case is not surprising when it is considered that the fluid in the separated region can only be removed at its own low velocity after boundary-layer reattachment becomes possible, while the boundary layer can separate from all points of the upper surface of the airfoil when stall occurs and fill the passage very rapidly. At the higher values of β_1, reversed flow was observed in the channels between airfoils after stall had occurred, so that, after the reverse flow had stopped, a small amount of initially stationary fluid had to be removed from the channel before good flow could recommence (figs. 22(c) and 23). It can be seen, therefore, that it is impossible to separate the effect of boundary-layer time delay from the inertia effect for measurement purposes during the unstalling process since the flow rate through the channel must be changed before the reattached boundary layer can be seen. On the other hand, when the airfoil stalls, flow separation and a decrease in α can take place without necessarily being accompanied by a change in flow rate through the channel, so that the time taken to stall after a change in inlet angle can be used to obtain an upper limit for the boundary-layer delay. The average time for stall was approximately 0.5 millisecond throughout the range of inlet angles; however, this is not equal to the boundary-layer time delay τ since, for the equivalent exponential-lag system, the minimum time required to attain 95 percent of the final change in α after a step change in β_1 would be 3τ. An approximate value for τ is therefore 0.16 millisecond. The inertia time constant L/c_3 was equal to 0.35 millisecond for this operating condition, since $c_3 = \frac{c_r}{\cos \beta_2} = 230$ fps and the blade chord $L = 0.96$ inch. Thus, the upper limit to the value of τ was approximately $\frac{1}{2}\frac{L}{c_3}$ and the true value was certainly smaller than this since the inlet angle did not change instantaneously and the observed response of the boundary layer was therefore slower than the theoretical response to a step change in inlet angle.

An interesting feature of the photographs is the occasional appearance after stall of what seem to be vortex planes at the entrance to a channel at the moment when the fluid within the channel is stationary and the unstalling process is about to commence (fig. 23). The planes retain their identity in subsequent pictures and move through the channel as good flow is reestablished. These planes may be formed by shear action between the deflected main flow and the stationary fluid within the passage and are visible as sharp lines only when they are perpendicular to the plane of the cascade.

Hot-wire equipment was used to check the number of stall cells and the propagation velocity and also for traversing in the spanwise direction to determine whether the whole passage was affected by rotating stall. The equipment employed was of the type manufactured by the Flow Corporation of Cambridge, Mass., and is shown in figure 24 with the dual-beam oscilloscope, Land camera, and audio-oscillator. Two hot-wire probes were installed behind the cascade at a distance apart of nine blade spacings. The signals from the probes were amplified, fed to the dual-beam Du Mont Type 322 oscilloscope, and photographed with a Land camera to be analyzed later. A time scale was added to each photograph by feeding an oscillatory signal to the beam intensity control of the oscilloscope and thus superimposing a line of blips of any desired frequency on the trace. Since the approximate number of stall cells was already known to be in the neighborhood of 12, two probes set a fixed distance apart were sufficient for determination of the phase lag and it was not necessary to resort to the more complex procedure required for identification of the number of stalls when no other information is available. From the phase-lag measurements, the number of stall cells could be calculated, and this information together with the frequency of the disturbances passing one wire was sufficient for computation of the propagation velocity. The accuracy of this method depends entirely on the regularity of the disturbances since the phase lag can be measured sufficiently closely to pinpoint the number of stall cells only if the phenomenon is periodic. As can be seen from the traces in figure 25, the variation between stall cells was responsible for an uncertainty of about one cell. For example, at $\beta_1 = 68^\circ$ the estimated number varied from 11 to 12, with 12 the most likely number. In addition, it is possible that the number of cells changed with time. In table I the results of the hot-wire measurements are compared with those obtained from schlieren photographs and the agreement is good. All the testing described in table I was carried out with a cascade Reynolds number of 240,000. By lowering the pressure at the inlet to the wind-tunnel compressors from 20 psia to 10 psia the Reynolds number was lowered to 120,000 without changing the Mach number and velocity. At the lower Reynolds number rotating stall did not begin until β_1 attained 63°, and the propagation velocity was approximately 15 percent lower than at the higher Reynolds number. There appeared to be 12 stall cells in the cascade. Since the Reynolds number should affect only the boundary-layer delay, and possibly the downstream pressure fluctuations, one would expect only a small change in propagation velocity with Reynolds number.

By traversing the passage with the hot-wire probes, the discovery was made that periodic rotating stall existed in a sharply defined band of about 1/4-inch depth adjacent to each end wall of the cascade while the disturbances were still of a random nature over the rest of the cascade. The tip stall began at $\beta_1 = 61^\circ$ and persisted until $\beta_1 = 63^\circ$, after which the periodic stall filled the cascade.

Removal of the boundary layer through the slots behind the nozzles had no measurable effect either on the rotating-stall characteristics of the cascade or on the curve of C_p versus β_1. If more than 2 percent of the main flow was removed, the cascade pressure rise decreased, indicating that fluid from outside the nozzle boundary layer was lost and that the inlet velocity to the cascade was reduced. The tip stall persisted and may have been caused by corner vortices being shed by the nozzles, as described in reference 10. Carbon-black patterns showed that the ends of the blades were stalled at $\beta_1 = 56^\circ$.

With increasing Mach number, the hot-wire pattern remained periodic until shock waves first appeared, after which a further increase in Mach number was followed by a rapid deterioration in the periodicity of the trace. A high-speed film taken at $\beta_1 = 67.2^\circ$ with $M_1 = 0.65$ showed the stall pattern building up and then collapsing as described below. Following a period of 14 milliseconds with all the airfoils stalled, a brief period of partial unstall moved across the window. Twenty-eight milliseconds later, 6 cycles of unstall moved past the window, each cycle occupying 1.5 milliseconds. After a further 20.7 milliseconds from the appearance of the cells, the cluster of stalls moved by once again, but there were now 8 of them apparently occupying one-half of the circle since they took 12 milliseconds to pass the window and had a propagation velocity of 184 fps, corresponding to a time of 21 milliseconds for 1 revolution. Another interval of 9-millisecond duration followed, with all the airfoils in the test window fully stalled, and at the end of this time the 8 cells came by again, but this time they had apparently sprung apart to fill the cascade since the interval between each cell had doubled. The film terminated at this point, but the hot-wire traces indicated that this process was typical of the phenomena at high Mach numbers and was probably followed by collapse and a later reforming of the pattern. A portion of the film is reproduced in figure 26 and shows strong lambda shocks appearing on the upper surface of the airfoils after the inlet angle increased, with boundary-layer separation behind the shock waves. At this Mach number V/c_r had a value of 0.66.

At very low Mach numbers the pressure fluctuations ahead of the cascade were three times as large as those behind the cascade (fig. 27). With increasing Mach number, the relative magnitude of the pressure fluctuations behind the cascade increased, until at $M_1 = 0.5$ they were as large as those ahead of the blades.

The nozzle wakes gave a useful indication of the inlet angle to the cascade during rotating stall, and a comparison of the high-speed motion pictures with the steady-flow schlieren photographs showed that during the unstalled portion of the cycle the inlet angle was never less than 56°, so that the airfoil was not operating to the left of the peak on the C_p curve at any time during the cycle.

No steady-state hysteresis effects were observed in the cascade response to changes in inlet angle, the pressure coefficient and rotating-stall characteristics being dependent only on β_1 and unaffected by the way in which the operating point was approached. This suggests that interference effects between blade rows are responsible for the hysteresis found in compressor stall characteristics.

Effect of cascade solidity on rotating stall.- With the original blade spacing, the stall cells had the appearance of a cloud of material of fixed identity rolling along the cascade. This illusion of continuity was so strong that, when the film was projected, the observer received the impression that the stall was flowing over and through the blades rather than being propagated from one blade to the next. The position of the boundary of the stall cell was a linear function of time and there was no appearance of discontinuity due to the finite blade spacing. In order to determine the effect of cascade solidity on the appearance, velocity, and number of the stalls, every second blade was removed from the cascade so that the solidity σ $\left(\text{defined as } \frac{\text{Chord}}{\text{Pitch}}\right)$ was reduced to 0.5, and the cascade was tested once again. In figure 28 the pressure coefficient is shown for values of π_m of 0.173 and 0.288, and in figure 29 β_2 is plotted against β_1. There was now very little turning of the flow and the greater part of the pressure rise was due to the change in radius, which was responsible for a theoretical pressure coefficient of 0.25. The C_p curve still showed the same characteristics as those observed with the higher solidity, with a dip in the curve at $\beta_1 = 49°$, a peak at $\beta_1 = 54°$, a minimum value at $\beta_1 = 60°$, and a second peak at $\beta_1 = 62°$. Rotating stall was observed in the wall boundary layer at the ends of the blades at an inlet angle of 61°, and full rotating stall commenced at 64°. The pressure coefficient and flow deflection were now too small to permit accurate measurement of α, which was approximately 0.9 when rotating stall began.

High-speed schlieren photographs taken with an inlet Mach number of 0.35 showed that the number of stall cells was approximately 13, with V/c_r increasing from 0.76 at $\beta_1 = 65°$ to 0.86 at $\beta_1 = 68.6°$. There were now only two airfoils in one wave length of the disturbance, and yet the stalls still moved with uniform velocity along the cascade. Flow separation on the suction surface of one blade commenced when the

pressure side of the blade was touched by the stalled region generated by the previous blade (figs. 30(a) and 30(b)). Frequently, the boundary layer reattached on one blade before stall commenced on the blade above it, so that part of the passage had good flow while the upper portion of the passage was still occupied by low-energy fluid. When a blade stalled, a region of flow separation appeared first at the leading edge and then grew and moved back along the blade, requiring approximately 0.5 millisecond to cover the blade. To obtain a better definition of the nozzle wakes, a high-speed motion picture was taken with an inlet Mach number of 0.45 (fig. 31) and, from this, it can be seen that the air inlet angle to an airfoil increased sharply just before the airfoil was touched by the stall propagating from the adjacent blade.

A further reduction in solidity to 0.33 was accomplished by removing nine of the remaining blades from the cascade. Only one blade was now visible in the window, but rotating stall still occurred and the turbulent air from the adjacent blade could be seen crossing the window before stall occurred on the blade in the window (fig. 32). The frequency of the disturbances was now almost twice the frequency obtained with a cascade solidity of unity, being 630 cps at $\beta_1 = 68.6^\circ$. Hot-wire measurements showed that there were still approximately 13 stall cells in the cascade, propagating with a velocity of 200 fps.

When nine of the remaining blades were removed (leaving nine blades in the cascade) rotating stall did not appear, and for inlet angles greater than 61° the flow separated from the leading edge as shown in figure 33. The stalling process was quite abrupt, with the separation point jumping suddenly from the 30-percent-chord position to the leading edge as β_1 was increased from 60° to 61°.

In figure 34, the frequency of the stalls is plotted against solidity for $\beta_1 = 68.6^\circ$ and $M_1 = 0.35$, and on the same diagram the frequency of eddy formation for a single airfoil (Von Kármán vortex street) as determined by Fage and Johansen (ref. 11) is shown. The formula for the eddy frequency of a plate or airfoil is $f = 0.155\frac{V}{b}$, where f is the frequency in cycles per second, V is the free-stream velocity in feet per second, and b is the component of chord normal to the free stream in feet. The stall frequency apparently tended towards the single-airfoil eddy frequency as the solidity was decreased. When the cascade solidity is too low to permit rotating stall, the airfoils shed eddies, and for the nine airfoils in the cascade an attempt was made to measure the eddy frequency. Accurate determination was difficult because of stream turbulence and because the hot-wire could not be traversed to find the position where the disturbances were most regular, but the eddy frequency appeared to be approximately 1,000 cps and this point lay on a smooth curve through the single-airfoil eddy frequency and the rotating-stall frequencies. Although accurate

determination of the eddy frequency was not possible with the present arrangement of the apparatus, this result suggests that there may be a connection between the eddy frequency in the absence of rotating stall and the frequency of stall cells with small wave lengths. No experimental work has apparently been done on the effect of blade spacing on eddy frequency and it would appear that such a study might shed some light on the relationship (if any) between eddy frequency and rotating stall. The eddy frequency is governed by the same parameters that determine the boundary-layer response in rotating stall and the fact that no satisfactory theory of vortex shedding has yet been developed is an indication of the complexity of the problem and the inadequacy of the simple exponential-lag representation of the boundary-layer response.

Comparison of theory with experiment.- Using the simple theory with τ assumed negligible, the theoretical propagation velocities were computed from the curves of C_p and β_2 versus β_1 for the cascade with solidities of 1 and 0.5. The calculations could be made only in the steady-flow region since it is unlikely that the pressure measurements in the rotating-stall region represent the steady cascade performance. In consequence, it is not possible to compare the theoretical propagation velocities directly with the experimental results for the same angles. In figure 35(a), the computed propagation velocities for 9, 10, 11, and 12 stalls are plotted versus β_1 for $\sigma = 1$, together with the experimental velocities. The broken lines represent the extrapolation of the theoretical curves into the rotating-stall regime and it can be seen that most of the experimental points lie within this area, which is as much as could be hoped for from a simple linearized theory. In this case, failure to consider the inertia of the fluid within the cascade would result in an error of the order of 100 percent in the predicted propagation velocity. The propagation velocity with a Reynolds number of 120,000 and 12 stall cells is slightly smaller than that with 12 cells and a Reynolds number of 240,000.

In figure 35(b), the computed and observed propagation velocities are shown for the lower solidity, and here the agreement is not so good. The assumption of one-dimensional flow within the passages is certainly not valid for low cascade solidity and the effective inertia of the air within the cascade may be considerably less than the value given by the theory. The good agreement between the experimental results and the simple theory for the high-solidity cascade suggests that the boundary-layer time delay τ may be considerably smaller than the approximate value calculated earlier, since a value of τ equal to $\frac{1}{2}\frac{L}{c_3}$ would reduce the predicted propagation velocity by about 30 percent. From figure 34, it can be seen that increasing the cascade solidity beyond 0.75 has little effect on the stall frequency and, hence, on the propagation velocity. Accordingly, it would appear that the neglect of finite blade spacing in the theory is justifiable for solidities greater than 0.75.

Rotating Stall in a Free-Vortex Single-Stage Axial-Flow Compressor

Some of the unpublished results obtained in an investigation of rotating stall in a single-stage compressor are presented herein for comparison with cascade performance and theory. The compressor was a free-vortex machine with a hub-tip ratio of 0.75, and the stage consisted of a row of inlet guide vanes, a rotor, and a set of stator blades. The axial clearance between the rotor and guide vanes was 1.5 inches and the rotor had an outside diameter of 23.25 inches and held 44 blades with a mean chord length of 1.5 inches. With the stator removed, an investigation of the rotating-stall characteristics of the machine was made using hot-wire equipment. For the rotor, the geometry of the blading was quite similar to that of the stationary cascade, with a design-point air inlet angle of 48° at the mean radius.

The performance of the rotor in terms of pressure coefficient and relative outlet angle at the mean radius versus relative inlet angle is shown in figures 36 and 37. As the mass flow was decreased at 1,500 rpm, eight stall cells appeared at $\beta_1 = 67^\circ$ covering the blades from root to tip and propagating at approximately 30 percent of rotor speed relative to the rotor. A further decrease in flow caused a change to nine cells at $\beta_1 = 71^\circ$, with approximately the same propagation speed. At $\beta_1 = 75^\circ$, the nine cells were replaced by a single stall cell propagating at 50 percent of rotor speed relative to the rotor. Three stall cells appeared at $\beta_1 = 80^\circ$ and four cells, at $\beta_1 = 84^\circ$. Throughout the whole rotating-stall range, the pressure fluctuations ahead of the inlet guide vanes were less than 25 percent of the pressure variations between the guide vanes and the rotor, indicating that the effect of the guide vanes on the unsteady flow was substantially as assumed in the analysis. The pressure variations behind the rotor caused by rotating stall (that is, the difference between the fluctuations with and without rotating stall) were less than 25 percent of those ahead of the rotor throughout the whole flow range in which rotating stall was obtained.

In figure 38, the predicted and observed values of propagation velocity are plotted against β_1. At the commencement of rotating stall where the linearized theory is most likely to be applicable, the agreement is remarkably good. As in the cascade, the accuracy of the simple theory indicates that the effect of the boundary-layer delay on velocity must be small. The change from nine cells to one cell at $\beta_1 = 75^\circ$ was accompanied by a considerable increase in propagation velocity, verifying the prediction that propagation velocity should increase with wave length. The theory comes within 25 percent in predicting the propagation velocities of the large stall cells, probably because the pressure fluctuations behind the rotor were small in this case even for large cells. By considering the flow field behind the cascade as a continuum, it is possible to obtain a solution for propagation velocity which reduces to the

Sears-Marble result for large waves with small pressure rise across the cascade (appendix C). This solution predicts propagation velocities which are much lower than the experimental values for both the stationary cascade and the rotor, showing that neglecting the downstream pressure fluctuations is the better assumption for the single blade rows tested.

SUMMARY OF RESULTS

A theory of stall propagation in a cascade of airfoils of high solidity has been developed which includes the effects of finite blade chord and of the boundary-layer response to changes in angle of attack. When the flow downstream of the blade row was treated as a series of free jets discharging into a constant pressure chamber, the following results were obtained:

(1) The wave length of the stall cells at the beginning of rotating stall, which was obtained analytically, was dependent on the amount of time required for movement of the separation point on the airfoil (boundary-layer time delay).

(2) The theoretical prediction that the velocity of stall propagation increases with the wave length of the stall cell was confirmed by experiment.

(3) The values obtained analytically for the stall propagation velocities agreed within 25 percent over a wide range of wave lengths with the results obtained experimentally on both the stationary circular cascade and the single-stage compressor.

When the flow downstream of the cascade was treated as a continuum, the solution for the stall propagation velocity applied to the case of large waves with a small pressure rise across the cascade. For this case the predicted stall propagation velocities were much lower than those obtained experimentally.

Massachusetts Institute of Technology,
Cambridge, Mass., May 10, 1955.

APPENDIX A

CALCULATION OF CASCADE DISCHARGE COEFFICIENT FOR REAL CASCADE

The cascade discharge coefficient α has been defined as the ratio of the actual mass flow through the cascade to the ideal mass flow for the same value of $(p_{o_1} - p_2)$ and flow deflection with no losses. It may be obtained from conventional test results as follows:

For a rectilinear cascade,

$$\alpha = \frac{\text{Actual mass flow}}{\text{Ideal mass flow for same } (p_{o_1} - p_2)}$$

Therefore,

$$\alpha = \frac{c_1 \cos \beta_1}{(c_2)_{\text{ideal}} \cos \beta_2}$$

$$= \frac{c_1 \cos \beta_1}{\cos \beta_2 \sqrt{\frac{2}{\rho}(p_{o_1} - p_2)}}$$

Since $p_{o_2} = p_{o_1}$ with no losses,

$$\alpha = \frac{c_1 \cos \beta_1}{\cos \beta_2 \sqrt{\frac{2}{\rho}\left[(p_{o_1} - p_1) - (p_2 - p_1)\right]}}$$

Thus,

$$\alpha = \frac{c_1 \cos \beta_1}{\cos \beta_2 \sqrt{c_1^2 - C_p c_1^2}}$$

$$= \frac{\cos \beta_1}{\cos \beta_2 \sqrt{1 - C_p}}$$

where

$$C_p = \left(p_2 - p_1\right) \Big/ \frac{\rho}{2} c_1^2$$

For a circular cascade,

$$\alpha = \frac{2\pi r_1 c_1 \cos \beta_1}{2\pi r_2 (c_2)_{ideal} \cos \beta_2}$$

which reduces to

$$\alpha = \frac{r_1}{r_2} \frac{\cos \beta_1}{\cos \beta_2 \sqrt{1 - C_p}}$$

APPENDIX B

STALL PROPAGATION VELOCITY IN POLAR COORDINATES

Stall Propagation in Circular Cascade

The circular cascade arrangement is as shown in figure 9. Consider disturbances from an incompressible plane source-vortex flow with velocity components $c_\theta = c_{\theta_1}\frac{r_1}{r}$ and $c_r = c_{r_1}\frac{r_1}{r}$ and angle β_1 measured from the radial direction. The flow before the cascade is irrotational so that a velocity potential can be used.

In the disturbed flow $u = c_{r_1}\frac{r_1}{r} + \varphi_r$ and $v = c_{\theta_1}\frac{r_1}{r} + \frac{1}{r}\varphi_\theta$. From continuity,

$$\frac{\partial}{\partial r}(ur) + \frac{\partial v}{\partial \theta} = 0$$

Therefore,

$$r\varphi_{rr} + \varphi_r + \frac{1}{r}\varphi_{\theta\theta} = 0$$

Solutions to this equation are obtained in the form

$$\varphi = \sum_{n=2}^{\infty}\left[a_n(t)\cos n\theta + b_n(t)\sin n\theta\right]r^n$$

satisfying the condition $\varphi_r = \varphi_\theta = 0$ at $r = 0$.

For $n = 1$, the velocity perturbation does not die out at the origin.

From Bernoulli's equation for unsteady flow,

$$(\varphi_t)_1 + c_1\delta c_1 + \delta p_1/\rho = 0$$

If inertia effects are neglected between (1) and (3) (fig. 9) then

$$c_1 \delta c_1 + \delta p_1/\rho = c_3 \delta c_3 + \delta p_3/\rho$$

so that

$$(\varphi_t)_1 + c_3 \, \delta c_3 + \delta p_3/\rho = 0$$

Inertia Effects Within Cascade

In order to obtain the inertia effects within the cascade, it is assumed that the blades are in the form of logarithmic spirals of small curvature (valid if r_2/r_1 is close to unity); thus, the momentum equation along the mean line of the passage (called the l-axis) can be written

$$\frac{\partial c}{\partial t} + c \frac{\partial c}{\partial l} + \frac{1}{\rho} \frac{\partial p}{\partial l} = 0$$

the same equation given for the rectilinear cascade. A similar process of integration gives the equation

$$L \frac{\partial}{\partial t}(\delta c_3) + (\varphi_t)_1 + c_2 \, \delta c_2 = 0$$

Also,

$$c_2 \, \delta c_2 = \left(\frac{A_3}{A_2}\right)^2 c_3 \, \delta c_3 - \left(\frac{A_3}{A_2}\right)^2 c_3^2 \frac{\delta A_2}{A_2}$$

as in the case of the rectilinear cascade. However, α is now given by $\alpha = \frac{r_1}{r_2} \frac{A_2}{A_3}$, since the outlet area with no separation region is now $\frac{r_2}{r_1} A_3$. Therefore,

$$c_2 \, \delta c_2 = \frac{1}{\alpha^2}\left(\frac{r_1}{r_2}\right)^2 c_3 \, \delta c_3 - \frac{1}{\alpha^2}\left(\frac{r_1}{r_2}\right)^2 c_3^2 \frac{\delta \alpha}{\alpha}$$

where

$$\frac{\delta\alpha}{\alpha} = \frac{\alpha'}{\alpha}\delta(u/v) = \frac{\alpha'}{\alpha}\frac{v\,du - u\,dv}{v^2}$$

which reduces to

$$\frac{\delta\alpha}{\alpha} = \frac{\alpha'}{\alpha}\frac{\varphi_r - \cot\beta_1\varphi_r/r}{c_{\theta_1}}$$

An equation for φ at (1) is obtained in the form

$$\frac{L}{\cos\beta_1}\varphi_{rt} + \frac{1}{\alpha^2}\left(\frac{r_1}{r_2}\right)^2\frac{c_r\varphi_r}{\cos^2\beta_1}\left(1 - \frac{\cot\beta_1\alpha'}{\alpha}\right) + \frac{\alpha'}{\alpha^3}\left(\frac{r_1}{r_2}\right)^2\frac{\cot^2\beta_1 c_r\varphi_\theta}{\cos^2\beta_2 r_1} = 0$$

By inserting the solution for φ and separating the coefficients of $\cos n\theta$ and $\sin n\theta$, two differential equations in terms of a_n and b_n are obtained which yield the characteristic equation

$$\left[\left(\frac{L}{\cos\beta_1} + r_1\right)\lambda_n + \frac{n}{\alpha^2}\left(\frac{r_1}{r_2}\right)^2\frac{c_{r_1}}{\cos^2\beta_1}\left(1 - \frac{\cot\beta_1\alpha'}{\alpha}\right)\right]^2 + \left[\frac{n\alpha'}{\alpha^3}\left(\frac{r_1}{r_2}\right)^2\frac{\cot^2\beta_1 c_{r_1}}{\cot^2\beta_2}\right]^2 = 0$$

Stall propagation occurs when $\alpha' = \frac{\alpha}{\cot\beta_1}$ and the velocity of the n^{th} harmonic is given by

$$\frac{V_n}{c_{r_1}} = \left(\frac{r_1}{r_2}\right)^2\frac{\cot\beta_1}{\alpha^2\cos\beta_2\left(\frac{lN}{r_1} + \cos\beta_2\right)}$$

Thus, if there are N symmetrical stall cells in the circular cascade, the velocity of propagation of the primary component is obtained from

$$\frac{V}{c_{r_1}} = \left(\frac{r_1}{r_2}\right)^2\frac{\cot\beta_1}{\alpha^2\cos\beta_2\left(\frac{lN}{r_1} + \cos\beta_2\right)}$$

Upstream Interference Effects

In determining upstream interference effects, if a row of inlet guide vanes is placed before the cascade, with outside radius R, then φ_r will be forced to zero at $r = R$ and a solution is obtained in the form

$$\varphi = \sum_{n=2}^{\infty} \left[a_n(t) \cos n\theta + b_n(t) \sin n\theta\right]\left(r^n + R^{2n}r^{-n}\right)$$

Substituting this solution, as before, in the differential equation satisfied by φ at (1) and carrying through the rest of the solution give

$$\frac{V}{c_{r_1}} = \left(\frac{r_1}{r_2}\right)^2 \frac{\cot \beta_1}{\alpha^2 \cos \beta_2 \left[\frac{LN}{r_1} \frac{1 - (R/r_1)^{2N}}{1 + (R/r_1)^{2N}} + \cos \beta_2\right]}$$

where V is the velocity of propagation of the fundamental component of the wave when there are N symmetric stall cells in the cascade.

APPENDIX C

STALL PROPAGATION VELOCITY WITH FLOW INTO A CONTINUUM

By assuming that the fluid from each blade passage mixes without pressure recovery immediately after leaving the cascade so that the downstream flow field is a continuum, it is possible to obtain an expression for propagation velocity which reduces to the Sears-Marble value for large waves with small pressure rise across the cascade.

Under these circumstances, the x-component of velocity immediately behind the cascade in the unsteady flow will be $c_x + (\varphi_x)_1$ and the y-component of velocity will be $\left[c_x + (\varphi_x)_1\right] \tan \beta_2$.

In the downstream flow field, let

$$u = c_x + u'$$

$$v = c_x \tan \beta_2 + v'$$

The linearized momentum equations are

$$\frac{1}{\rho} \frac{\partial}{\partial x}(\delta p) + \frac{\partial u'}{\partial t} + c_x \frac{\partial u'}{\partial x} + c_x \frac{\partial u'}{\partial y} \tan \beta_2 = 0$$

$$\frac{1}{\rho} \frac{\partial}{\partial y}(\delta p) + \frac{\partial v'}{\partial t} + c_x \frac{\partial v'}{\partial x} + c_x \frac{\partial v'}{\partial y} \tan \beta_2 = 0$$

Differentiating the x-momentum equation with respect to x and the y-momentum equation with respect to y and adding give (by using the continuity relation $\frac{\partial u'}{\partial x} + \frac{\partial v'}{\partial y} = 0$)

$$\frac{\partial^2}{\partial x^2}(\delta p) + \frac{\partial^2}{\partial y^2}(\delta p) = 0$$

A solution to this equation may be obtained in the form

$$\frac{\delta p}{\rho} = \sum_{n=1}^{\infty}\left[c_n(t)\ \cos\frac{n\pi y}{b} + d_n(t)\ \sin\frac{n\pi y}{b}\right]e^{-n\pi x/b}$$

From the x-momentum equation

$$\frac{1}{\rho}\frac{\partial}{\partial x}(\delta p) + \frac{\partial u'}{\partial t} + c_x\frac{\partial u'}{\partial x} + c_x \tan\beta_2\frac{\partial u'}{\partial y} = 0$$

But

$$\frac{\partial u'}{\partial x} + \frac{\partial v'}{\partial y} = 0$$

Therefore,

$$\frac{1}{\rho}\frac{\partial}{\partial x}(\delta p) + \frac{\partial u'}{\partial t} - c_x\frac{\partial v'}{\partial y} + c_x \tan\beta_2\frac{\partial u'}{\partial y} = 0$$

At the cascade,

$$v_2' = u_2' \tan\beta_2$$

Therefore,

$$\frac{1}{\rho}\frac{\partial}{\partial x}(\delta p_2) = -\frac{\partial u_2'}{\partial t}$$

but

$$-\frac{\partial u_2'}{\partial t} = \frac{\partial}{\partial x}(\varphi_x)_1 = -\frac{n\pi}{b}\sum_{n=1}^{\infty}\left(\frac{da_n}{dt}\cos\frac{n\pi y}{b} + \frac{db_n}{dt}\sin\frac{n\pi y}{b}\right)$$

and so

$$\frac{1}{\rho}\frac{\partial}{\partial x}(\delta p_2) = -\frac{n\pi}{b}\sum_{n=1}^{\infty}\left[c_n(t)\cos\frac{n\pi y}{b} + d_n(t)\sin\frac{n\pi y}{b}\right]$$

Therefore,

$$c_n(t) = \frac{da_n}{dt}$$

$$d_n(t) = \frac{db_n}{dt}$$

and $\delta p/\rho$ after the cascade is $\delta p_2/\rho$ which may be written as

$$\frac{\delta p_2}{\rho} = \frac{d}{dt}\left\{\sum_{n=1}^{\infty}\left[a_n(t)\cos\frac{n\pi y}{b} + b_n(t)\sin\frac{n\pi y}{b}\right]\right\}$$

$$= (\varphi_t)_1$$

By substituting this value for $\delta p_2/\rho$ in equation (5) instead of putting $\delta p_2 = 0$, the final expression for propagation velocity is

$$\frac{V}{c_x} = \frac{2(1 - C_p)}{\sin 2\beta_1\left(\frac{L\pi}{b\cos\beta_2} + 2\right)}$$

and this reduces to the Sears-Marble value for $C_p = 0$ and $L/b = 0$.

REFERENCES

1. Cheshire, L. J.: The Design and Development of Centrifugal Compressors for Aircraft Gas Turbines. Proc. Institution Mech. Eng. (London), vol. 153, 1945, pp. 426-440.

2. Emmons, H. W., Pearson, C. E., and Grant, H. P.: Compressor Surge and Stall Propagation. Advance Paper No. 53-A-65, A.S.M.E., Dec. 1953.

3. Iura, T., and Rannie, W. D.: Experimental Investigations of Propagating Stall in Axial-Flow Compressors. Trans. A.S.M.E., vol. 76, no. 3, Apr. 1954, pp. 463-471.

4. Huppert, M. C., and Benser, W. A.; Some Stall and Surge Phenomena in Axial-Flow Compressors. Jour. Aero. Sci., vol. 20, no. 12, Dec. 1953, pp. 835-845.

5. Sears, W. R.: A Theory of "Rotating Stall" in Axial-Flow Compressors. Contract AF-33(038)21406, Office Sci. Res., Dept. Air Force, and Graduate School Aero. Eng., Cornell Univ., Jan. 1953.

6. Marble, F. E.: Propagation of Stall in a Compressor Blade Row. Tech. Rep. No. 4, Contract AF-18(600)-178, Office Sci. Res., Dept. Air Force, and Daniel and Florence Guggenheim Jet Propulsion Center, C.I.T., Jan. 1954.

7. Stenning, Alan H.: Stall Propagation in Cascades of Airfoils. Readers' Forum, Jour. Aero. Sci., vol. 21, no. 10, Oct. 1954, pp. 711-713.

8. Kriebel, A. R.: Stall Propagation in Cascades of Airfoils. M. S. Thesis, Dept. Mech. Eng., M.I.T., June 1954.

9. Kriebel, A. R., and Stenning, A. H.: A Cascade Tunnel for Investigation of Rotating Stall. Rep. No. 26, Gas Turbine Lab., M.I.T., Aug. 1954.

10. Herzig, Howard Z., Hansen, Arthur G., and Costello, George R.: A Visualization Study of Secondary Flows in Cascades. NACA Rep. 1163, 1954. (Supersedes NACA TN 2947.)

11. Fage, A., and Johansen, F. C.: On the Flow of Air Behind an Inclined Flat Plate of Infinite Span. Proc. Roy. Soc. (London), ser. A., vol. 116, no. 773, Sept. 1, 1927, pp. 170-197.

TABLE I

COMPARISON OF PROPAGATION VELOCITIES

[Total temperature, 535° R; cascade Reynolds number, 240,000]

β_2, deg	M_1	c_{r1}, fps	Schlieren photographs			Hot-wire method		
			Number of stalls, N	Propagation velocity, V, fps	V/c_{r1}	Number of stalls, N	Propagation velocity, V, fps	V/c_{r1}
63.8	0.326	161	9	104	0.64	9	99	0.62
65.5	.343	160	10	110	.69	9	112	.70
67.2	.361	159	11	117	.74	11	116	.74
68.5	.377	159	--	---	----	12	115	.72

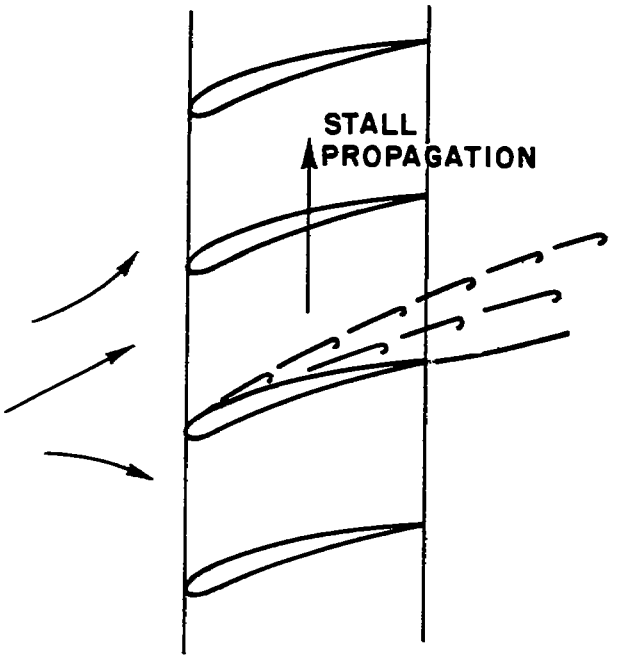

Figure 1.- Effect of stalled blade on flow entering cascade.

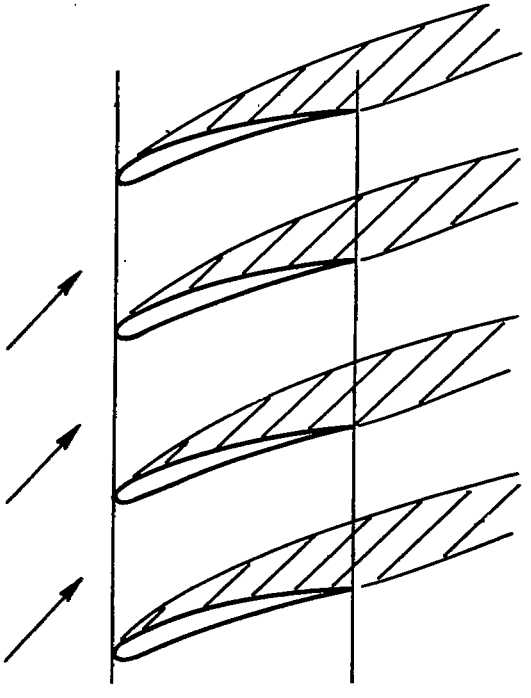

Figure 2.- Flow field of stalled cascade.

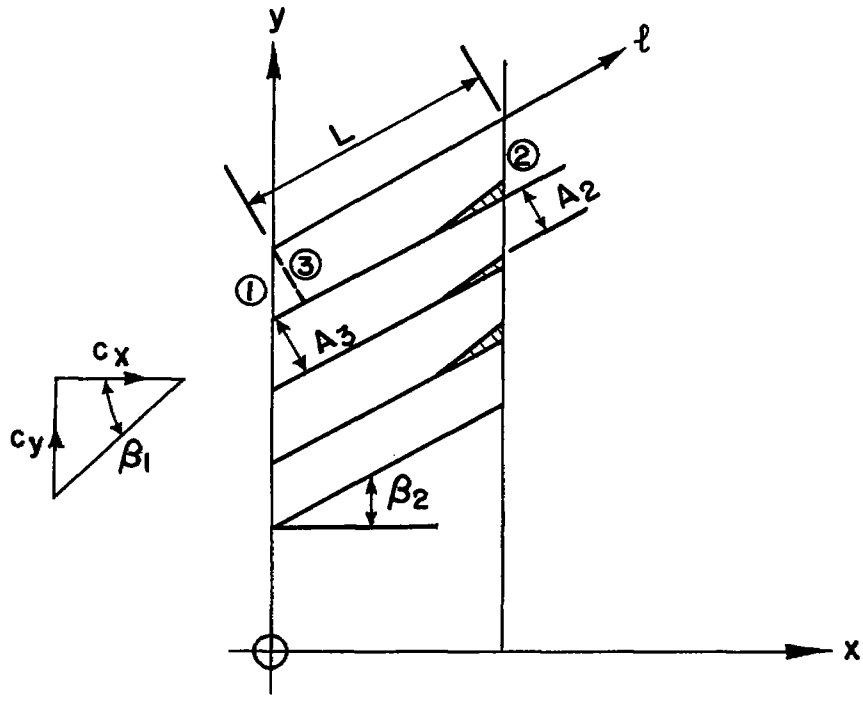

Figure 3.- Cascade representation and notation.

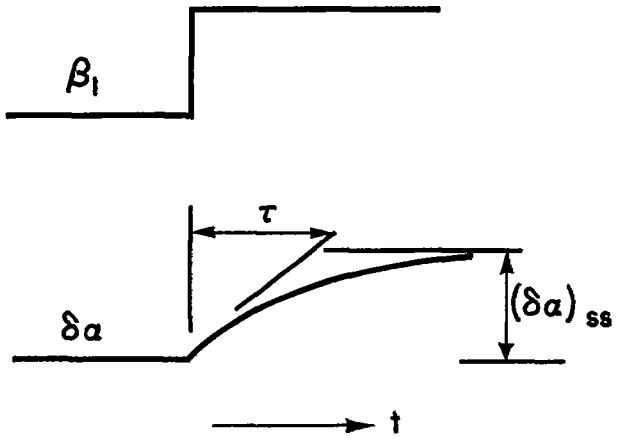

Figure 4.- Assumed boundary-layer response to step changes in β_1.

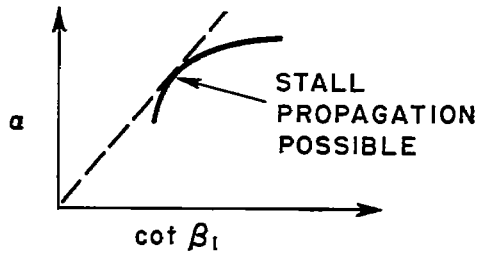

Figure 5.- Stability criterion for stall propagation.

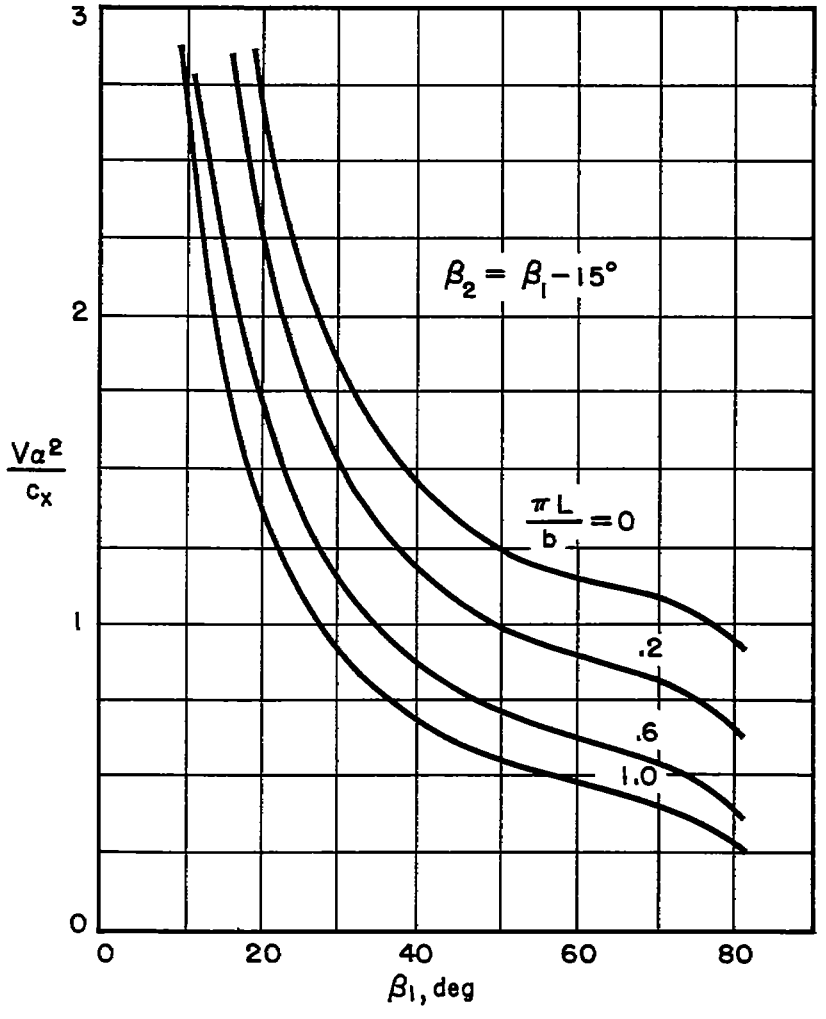

(a) 15° turn.

Figure 6.- Plot showing $\frac{Va^2}{c_x}$ versus β_1 for cascades in stalled condition.

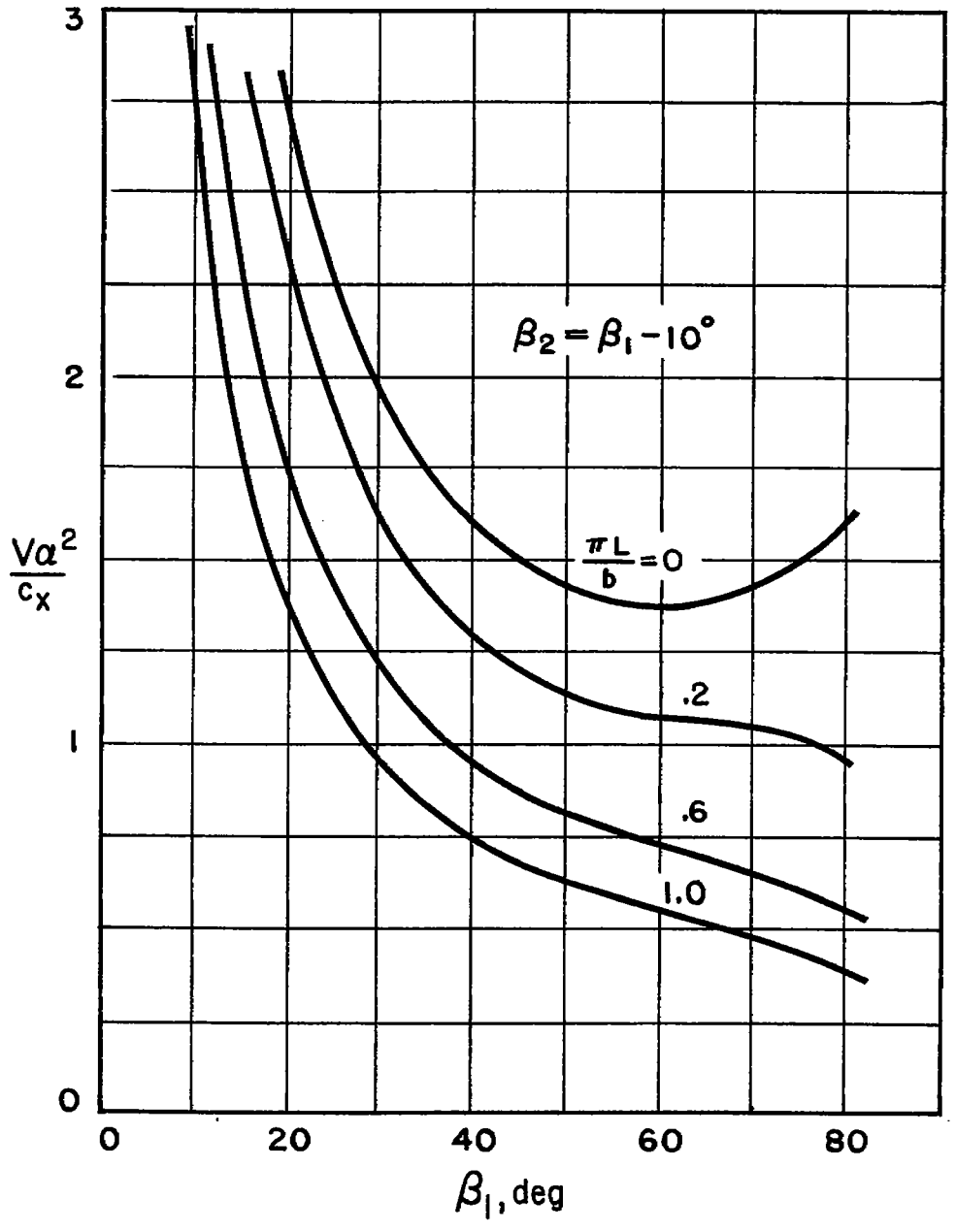

(b) 10° turn.

Figure 6.- Concluded.

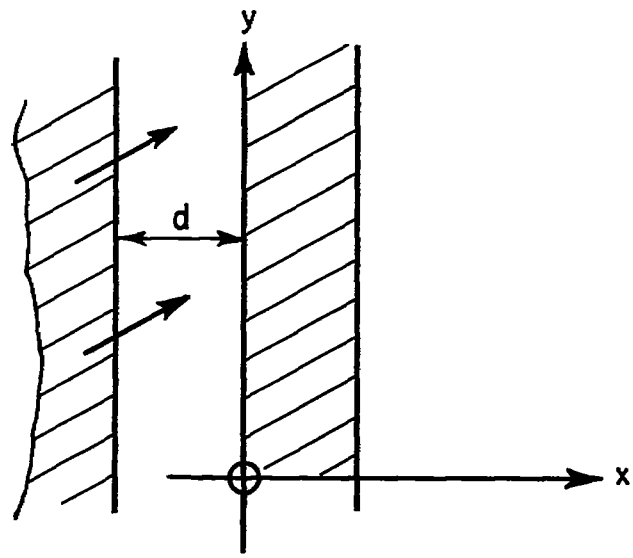

Figure 7.- Representation of cascade with inlet guide vanes.

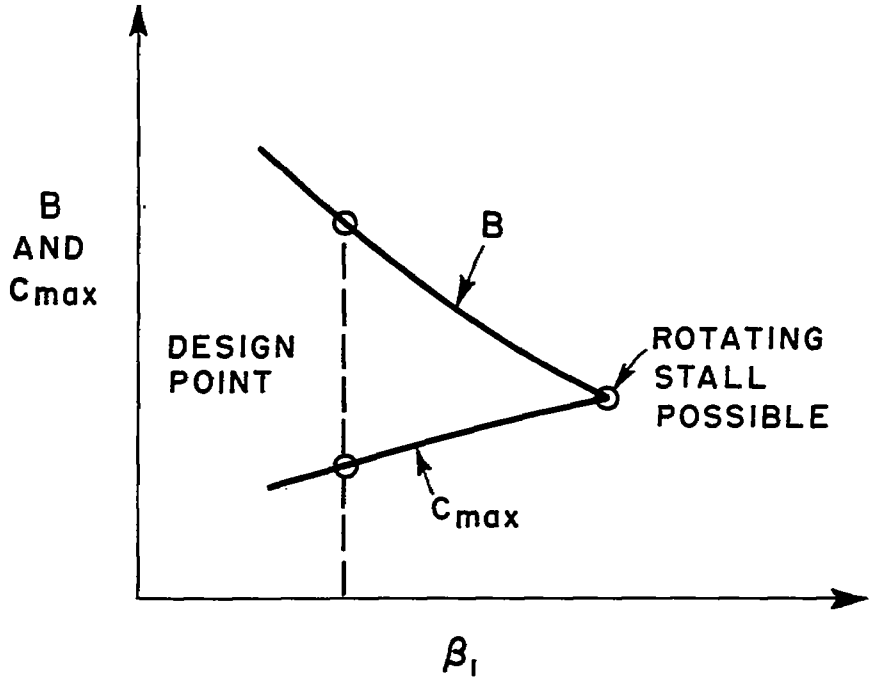

Figure 8.- Stability criterion with boundary-layer delay.

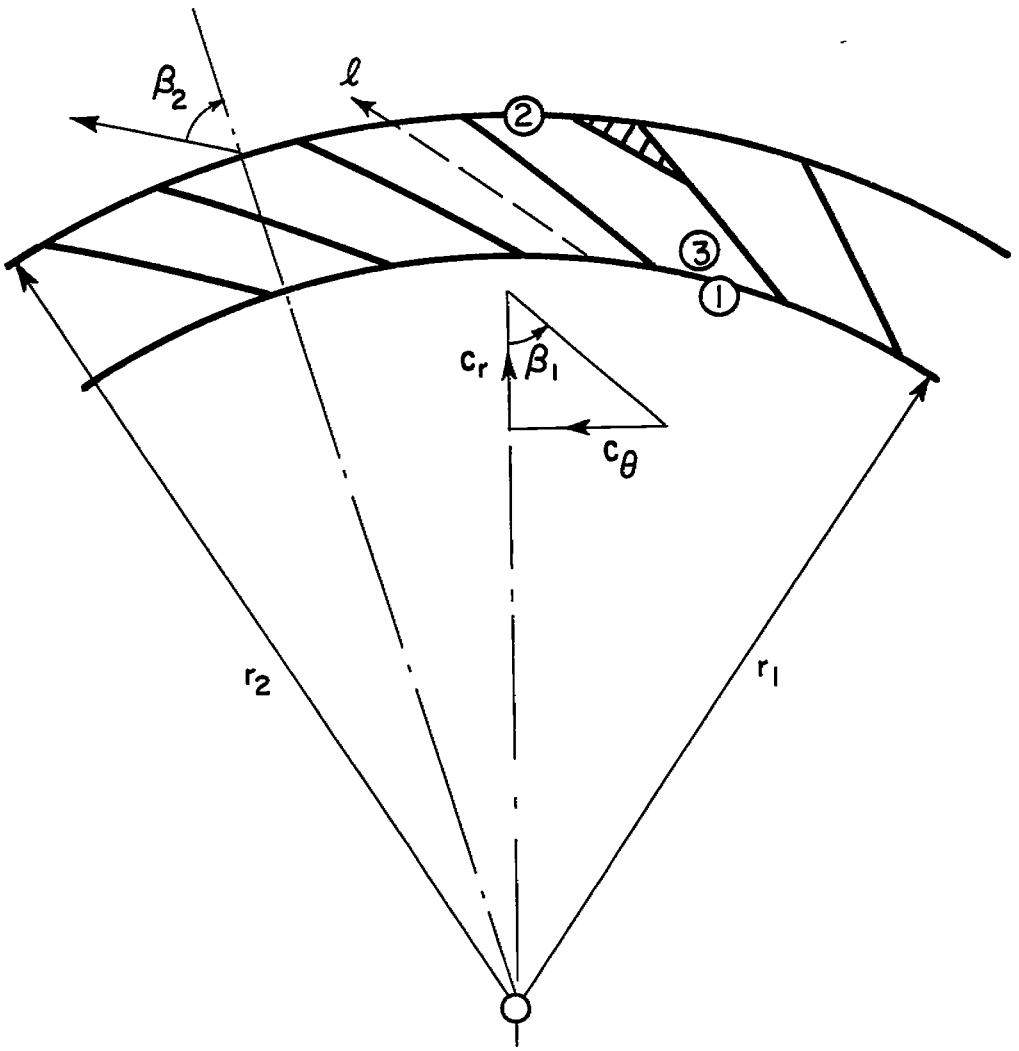

Figure 9.- Representation of circular cascade.

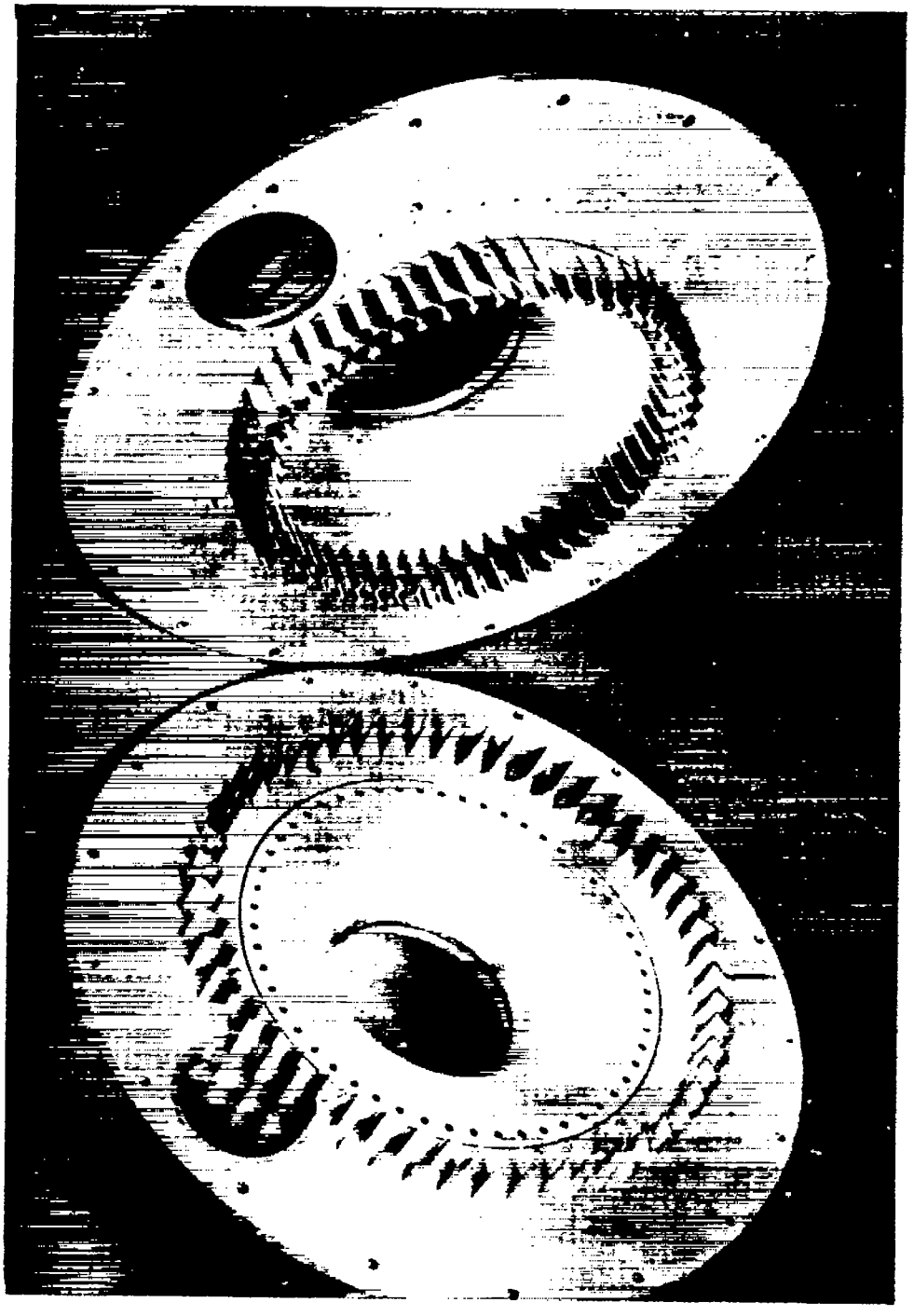

Figure 10.- Test section blading. L-92404

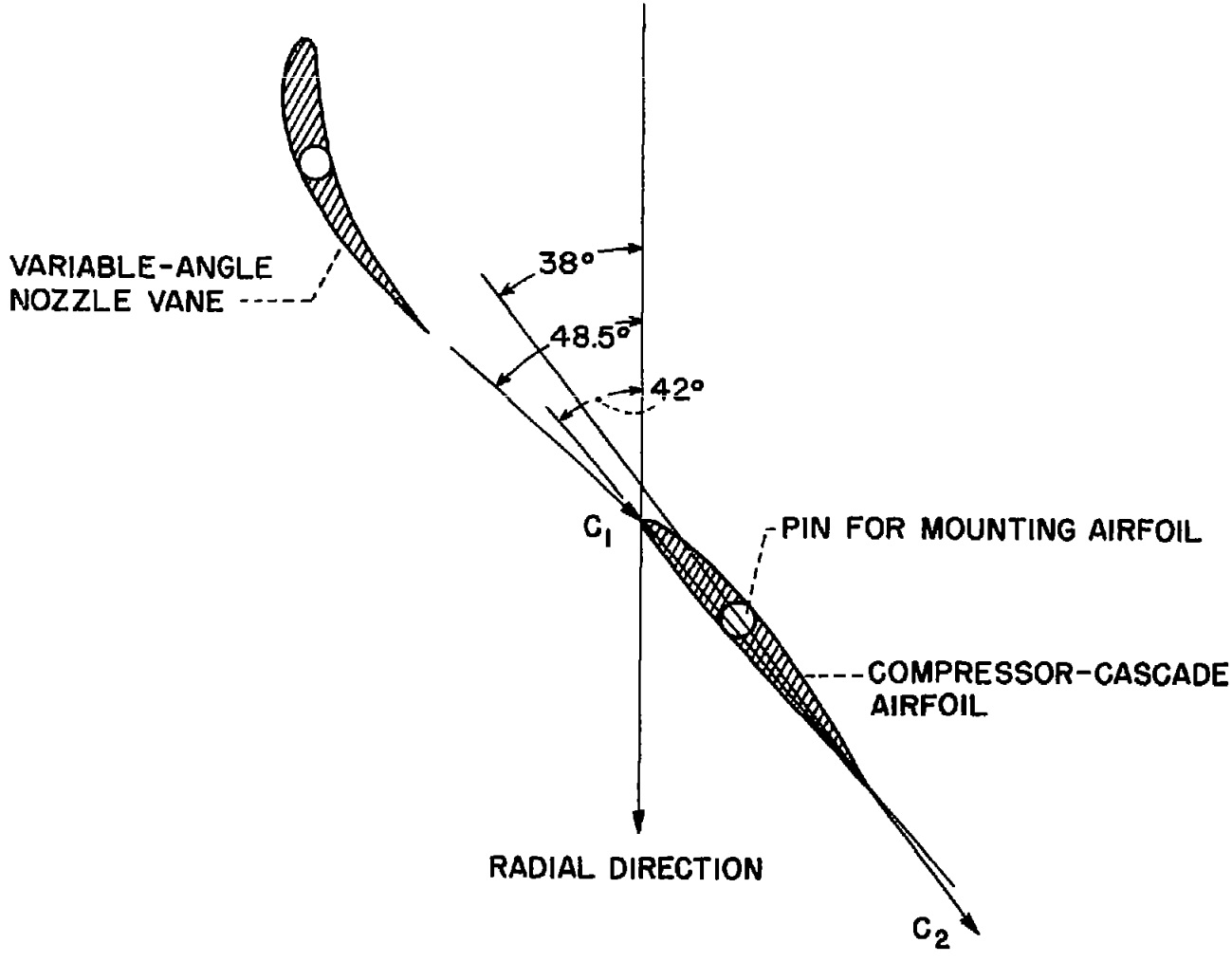

Figure 11.- Schematic blading diagram for stationary circular cascade showing design angles.

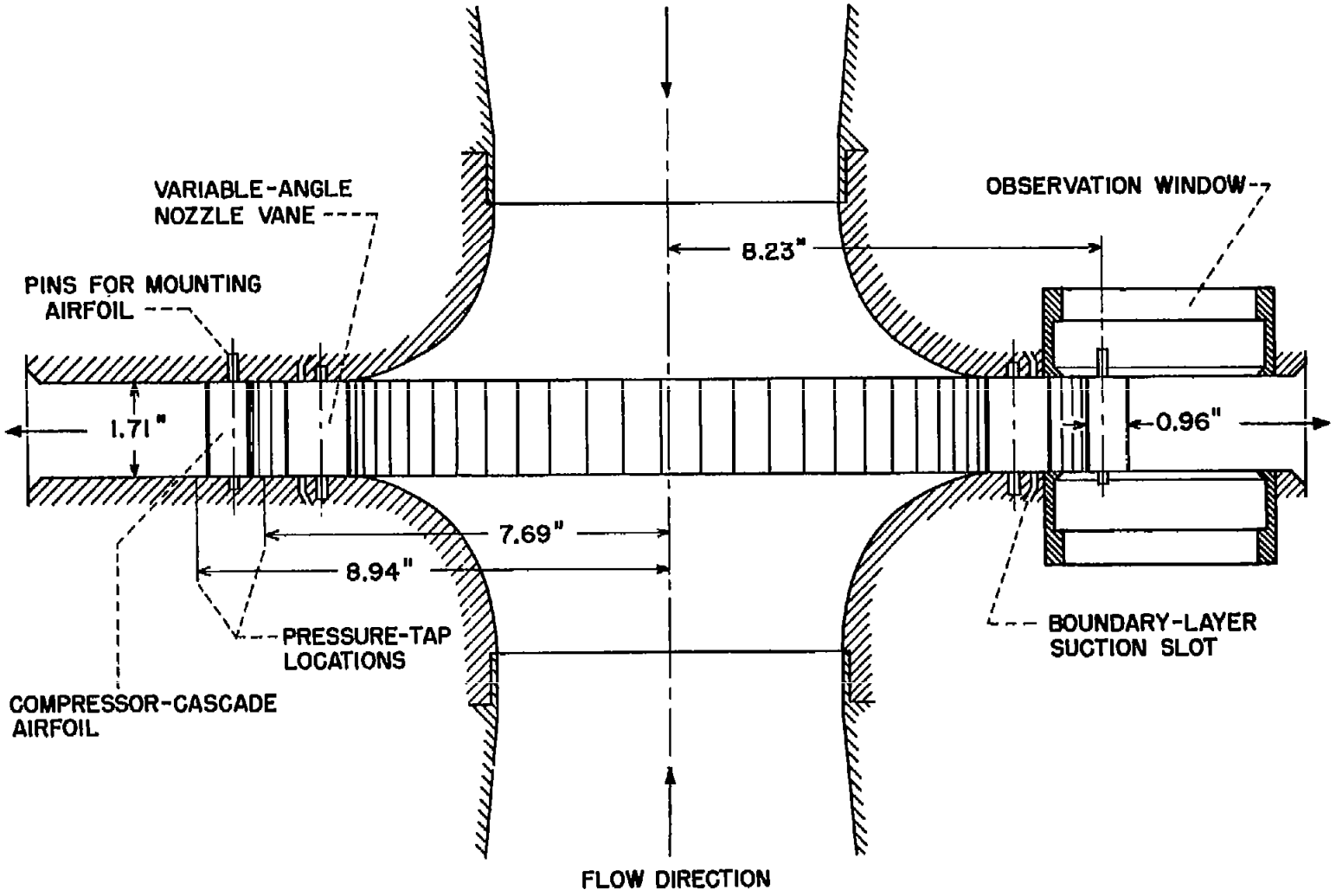

Figure 12.- Schematic diagram of stationary-circular-cascade test section.

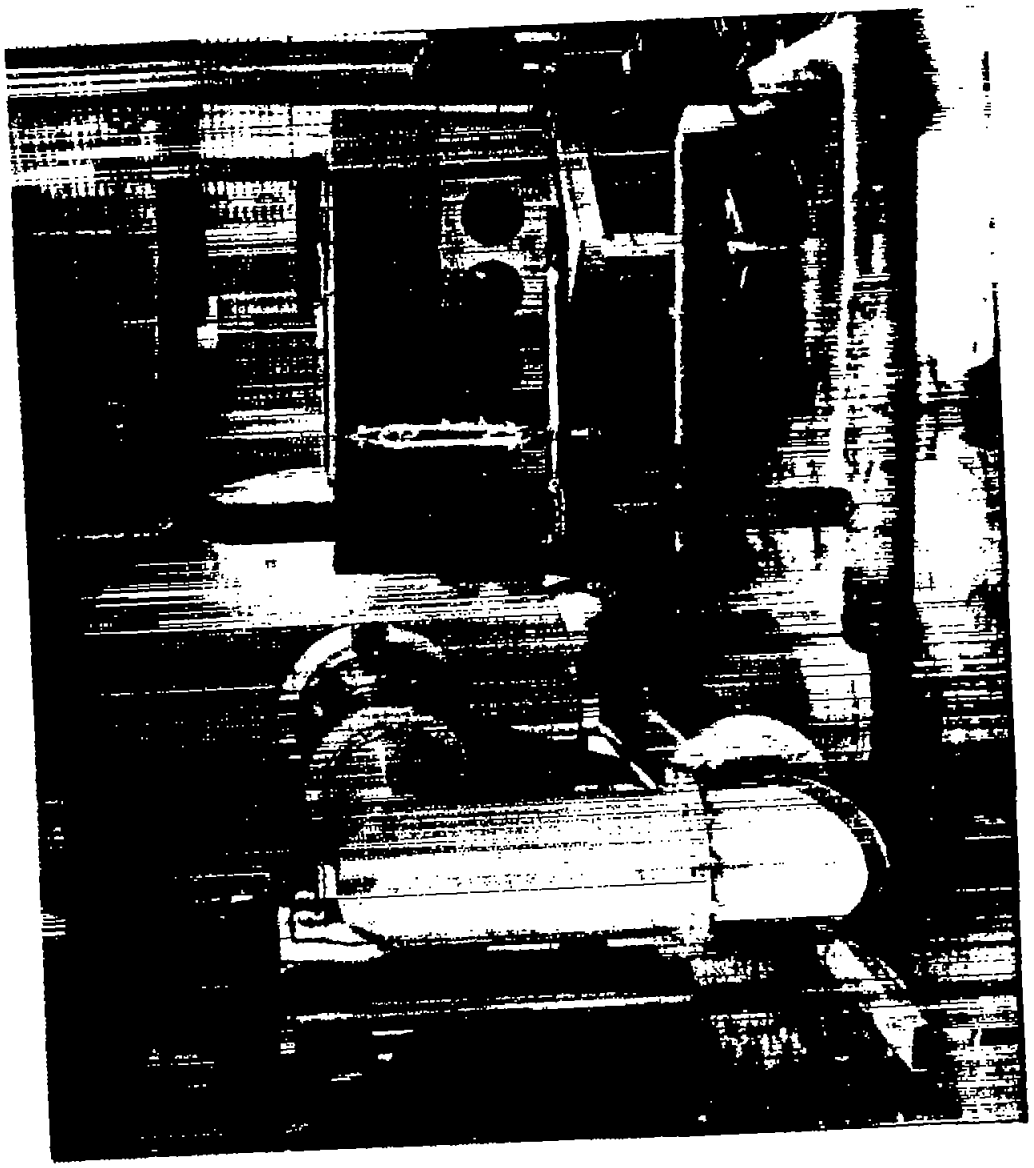

L-92405

Figure 13.- Cascade tunnel and portable schlieren.

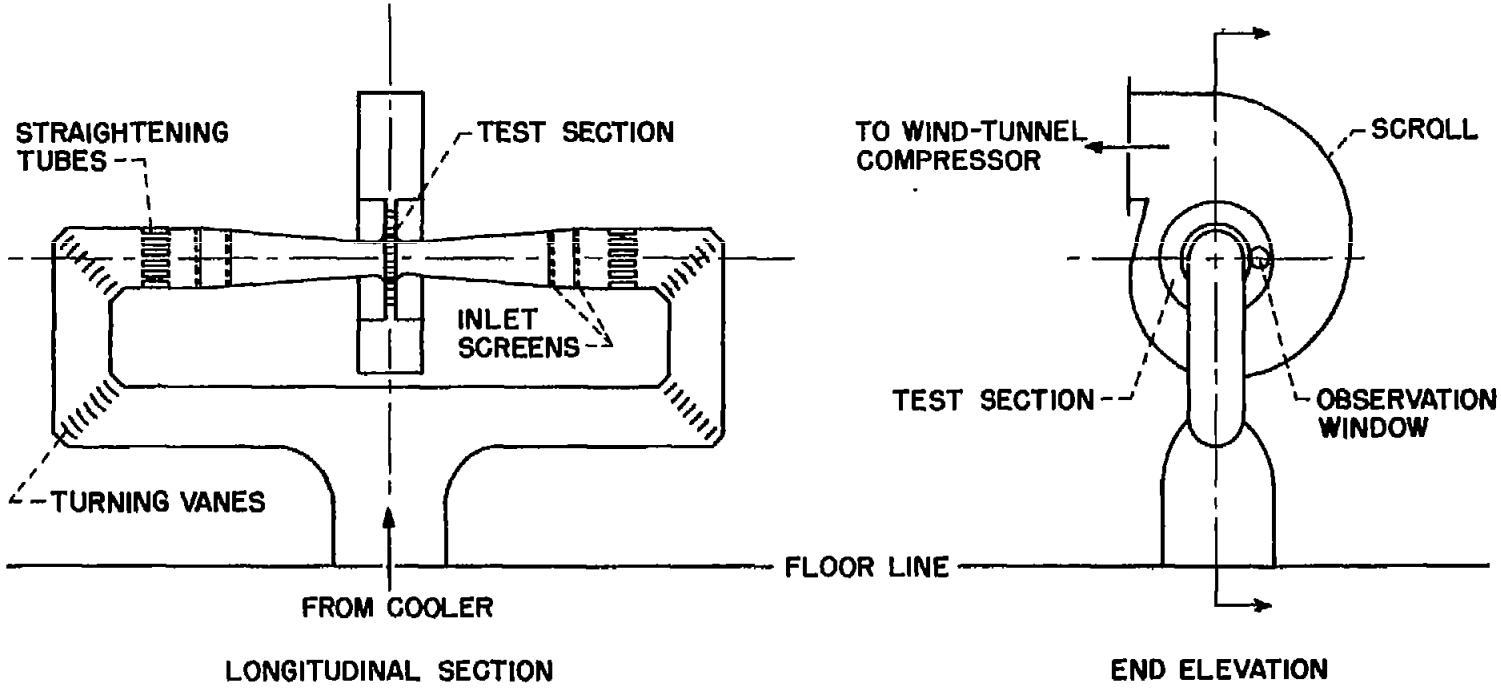

Figure 14.- Longitudinal section and end elevation of stationary-circular-cascade test facility.

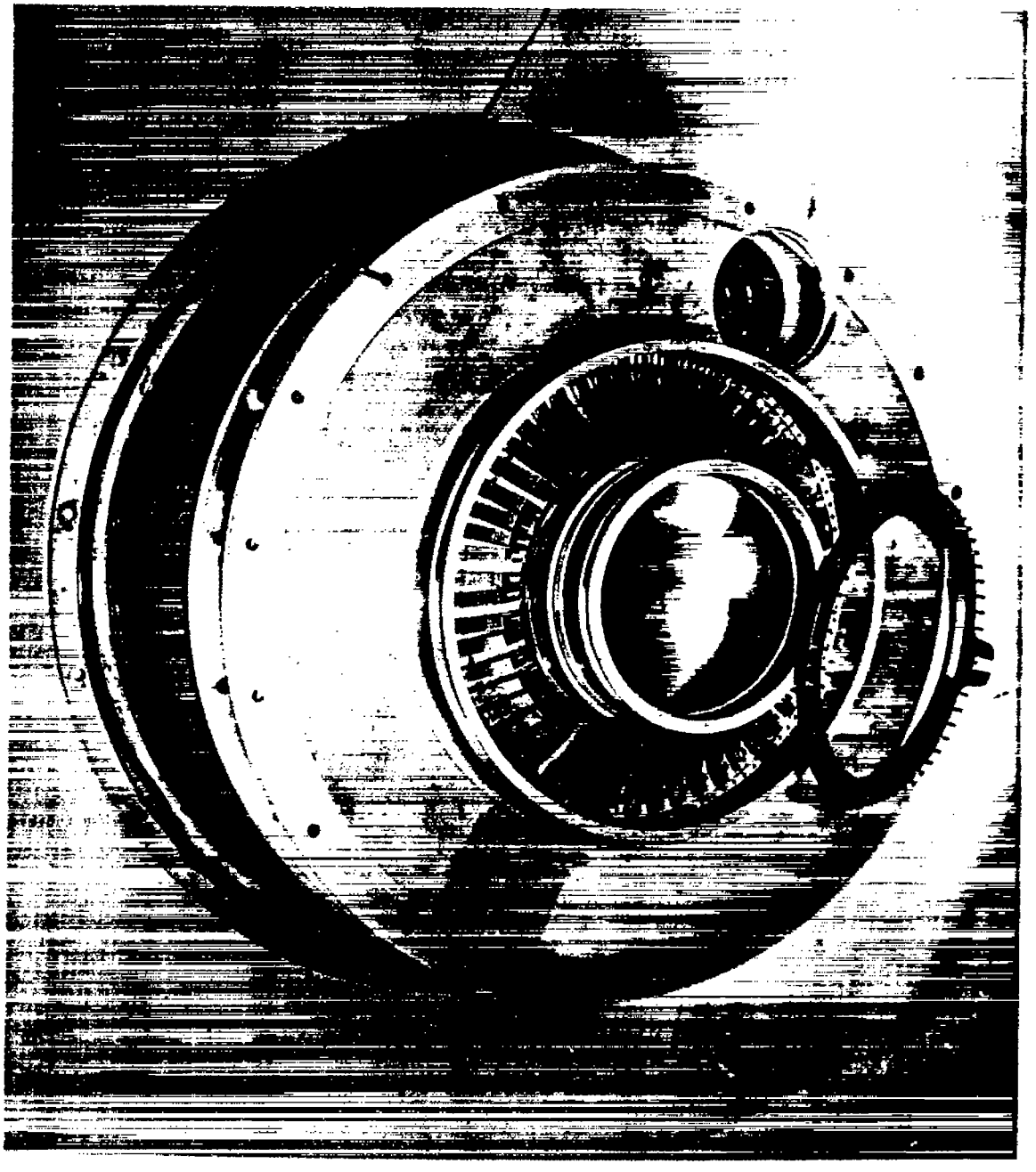

L-92406

Figure 15.- Test section of the stationary-circular-cascade tunnel.

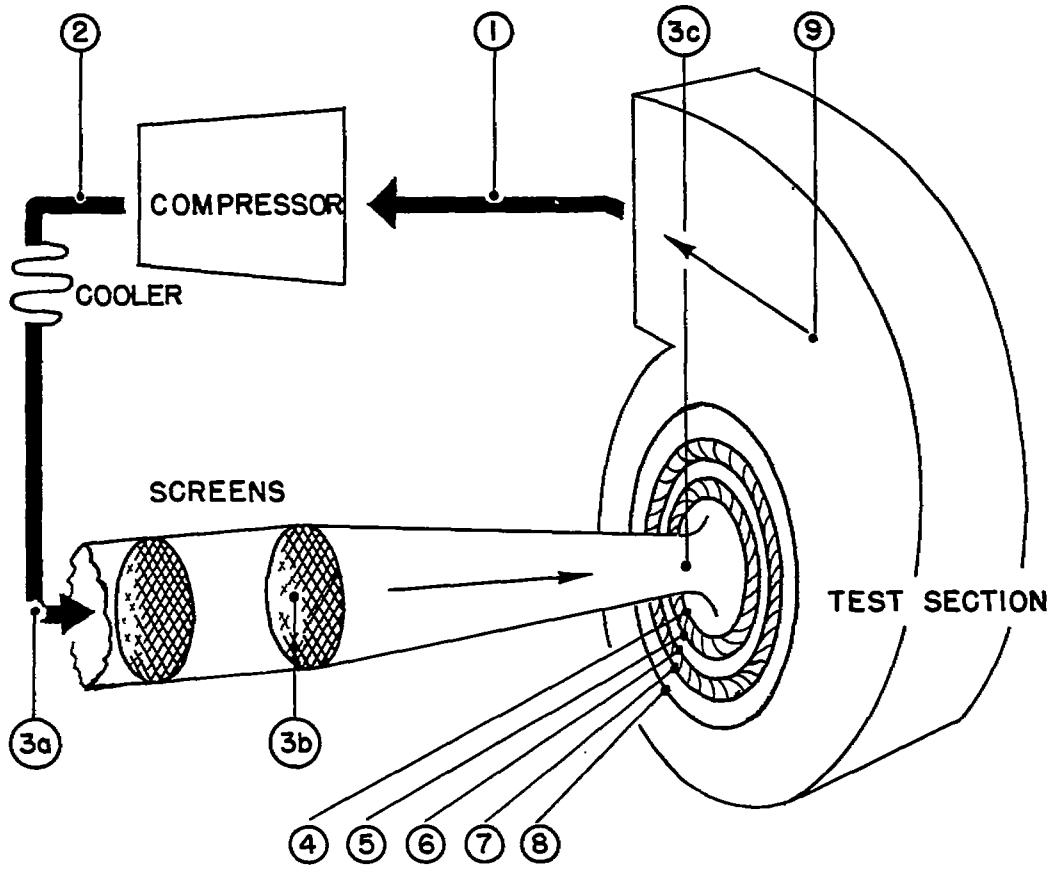

Station	Radius, in.	Mach number	Velocity, f p s	ρ_o, $\frac{lb}{ft^3}$	ρ	p_o, psia	p	T, °F
1			78	0.0712	0.0710	14.54	14.49	90
2			62	.0855	.0854	18.09	18.06	90
3a			127	.0814	.0809	16.60	16.47	89
3b			133	.0786	.0781	16.01	15.86	89
3c		0.44	498	.0786	.0715	16.01	14.02	70
4	6.0	.45	509	.0786	.0714	16.01	13.93	68
5	7.2	.71	776	.0771	.0608	15.69	11.25	45
6	7.9	.59	658	.0771	.0652	15.69	12.40	54
7	8.7	.39	443	.0759	.0703	15.47	13.93	73
8	12.0	.28	317	.0759	.0730	15.47	14.56	82
9	23.0	.10	115	.0714	.0711	14.56	15.86	89

Figure 16.- Schematic diagram of air circuit and tabulated properties.

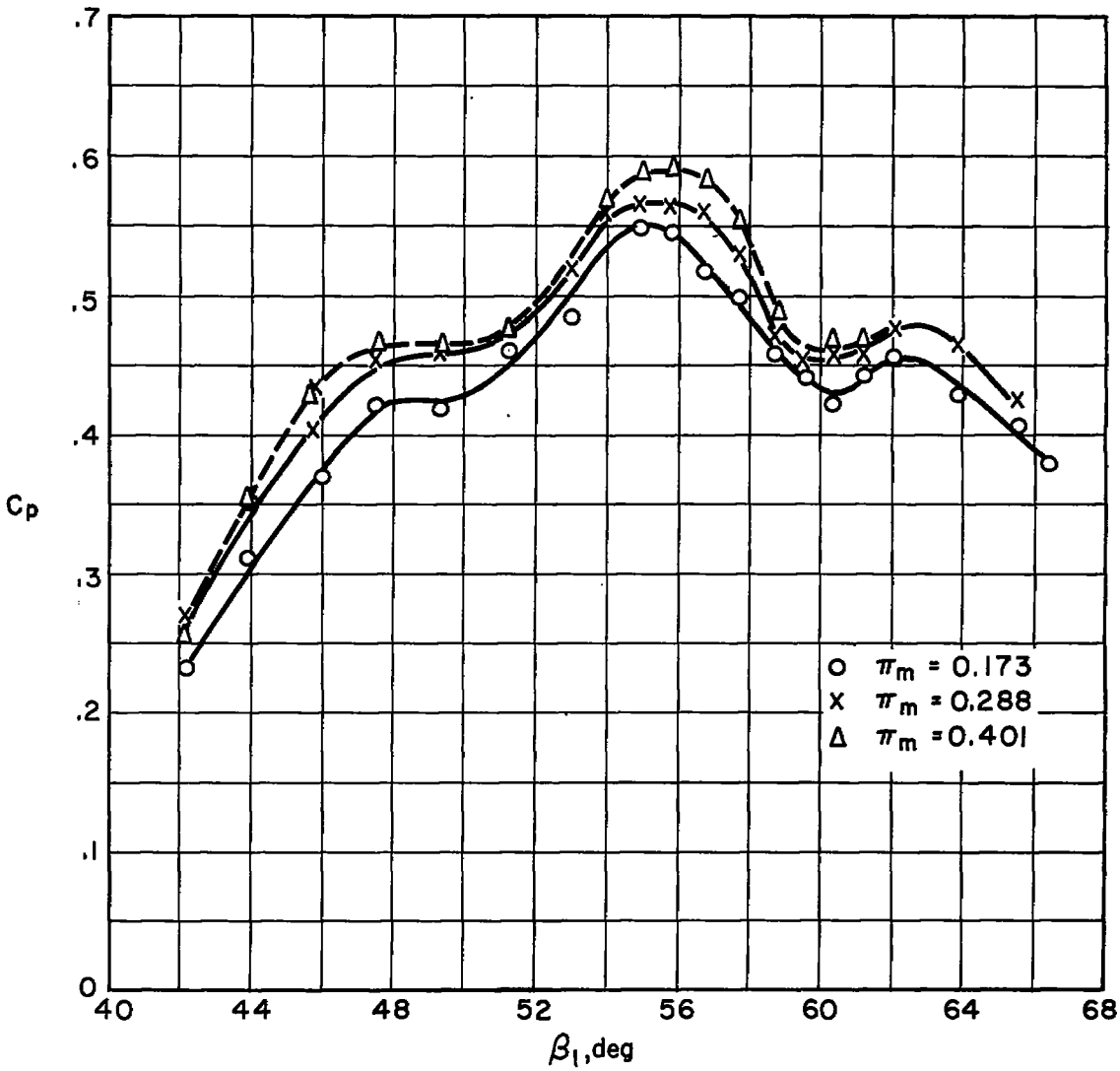

Figure 17.- Cascade performance. Pressure coefficient versus β_1 for $\sigma = 1.0$.

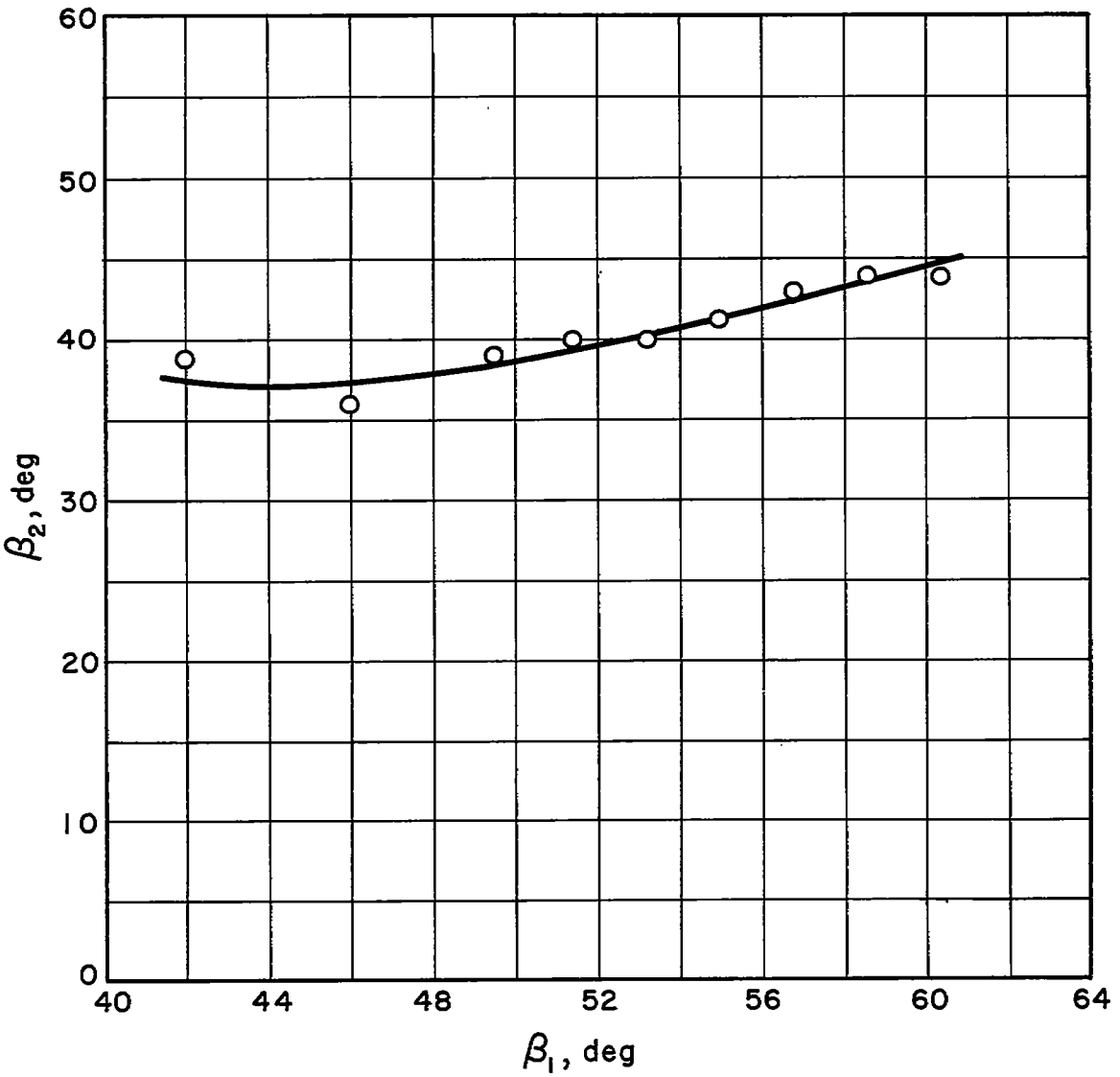

Figure 18.- Cascade performance. β_2 versus β_1 for $\sigma = 1.0$.

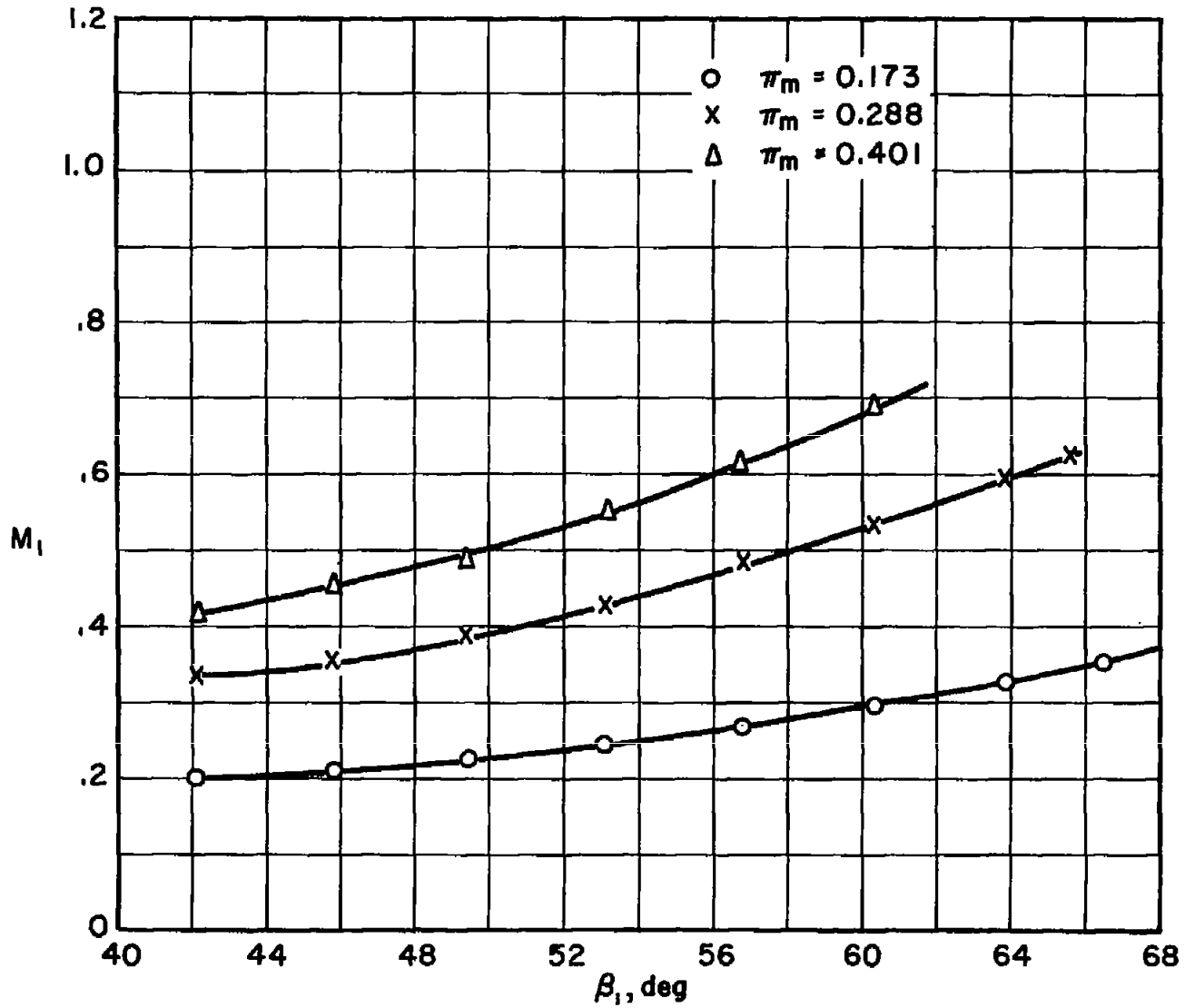

Figure 19.- Mach number entering cascade versus β_1.

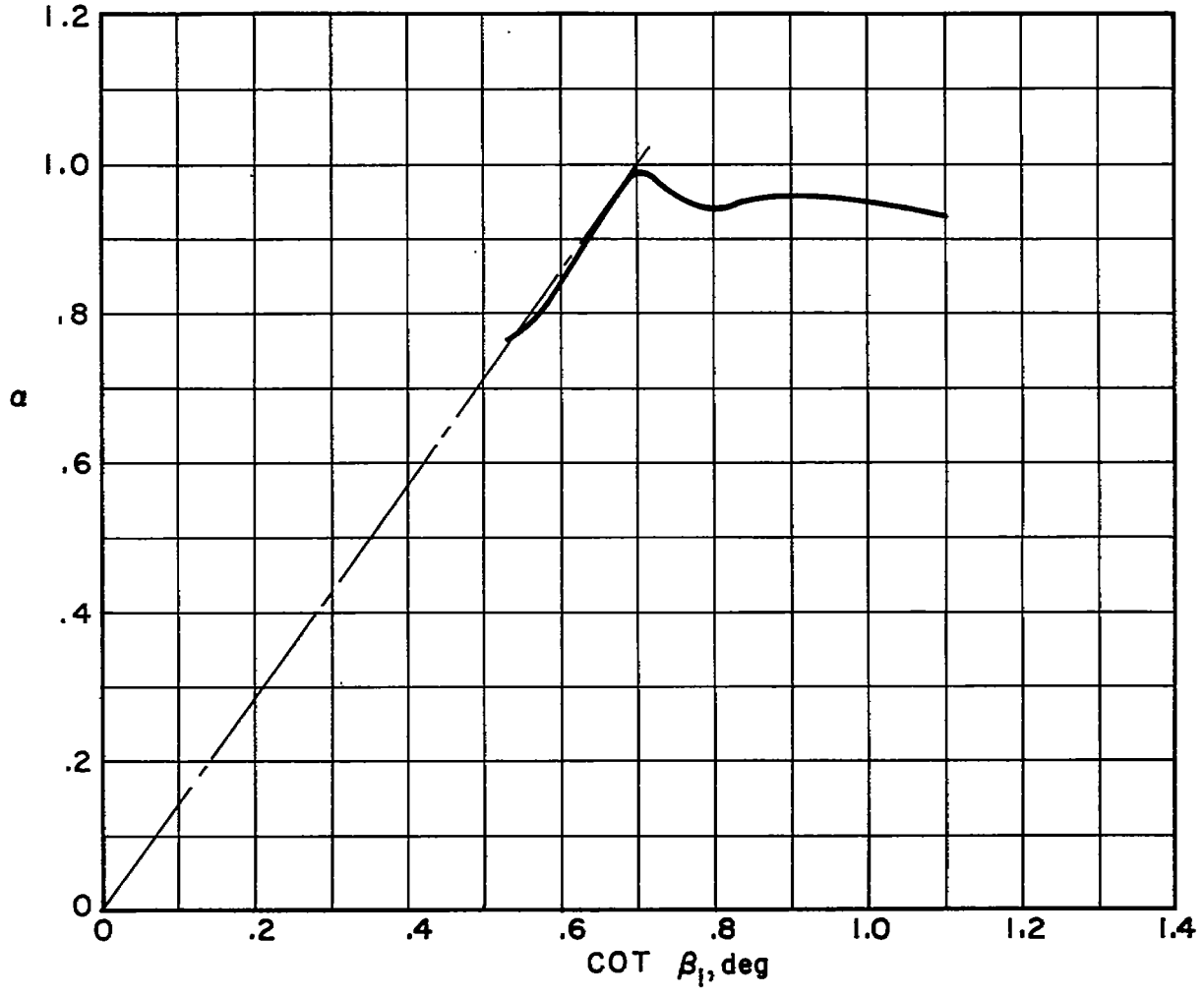

Figure 20.- Cascade performance. α versus cot β_1 for $\sigma = 1.0$. Broken line indicates gradient predicted by theory at the point where rotating stall begins.

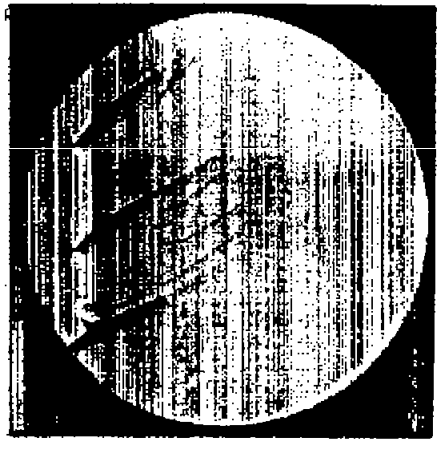

(a) $\beta_1 = 42°$.

(b) $\beta_1 = 46°$.

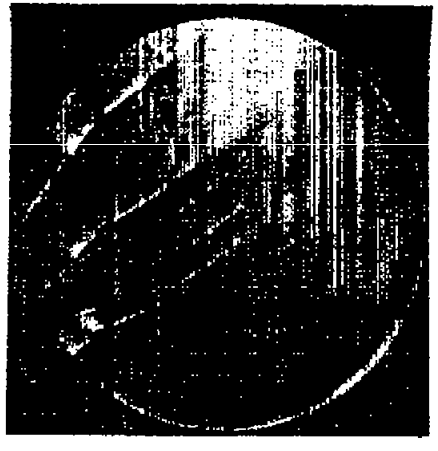

(c) $\beta_1 = 49.5°$.

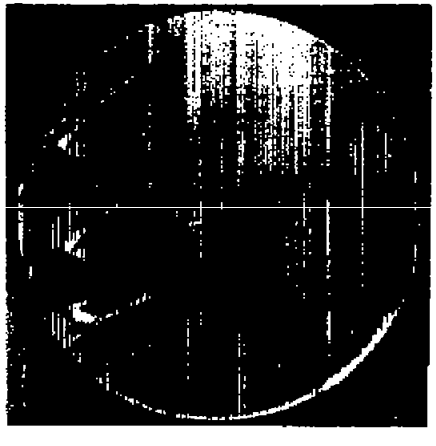

(d) $\beta_1 = 53.2°$.

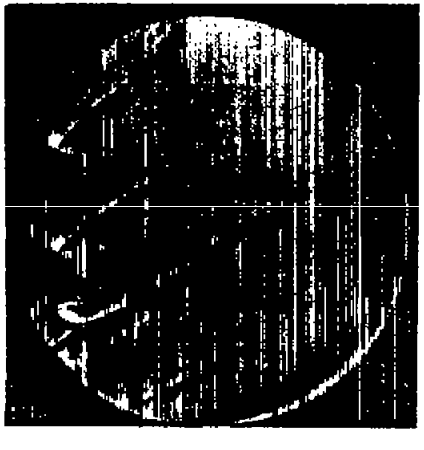

(e) $\beta_1 = 56.8°$.

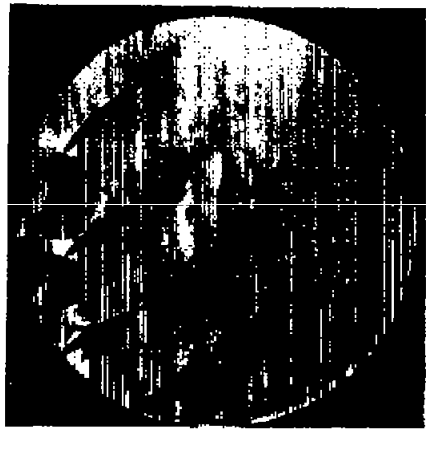

(f) $\beta_1 = 60.4°$.

L-92407

Figure 21.- Schlieren photographs of cascade in steady flow.

TIME

(a) $\beta_1 = 63^\circ$; $M_1 = 0.32$; $\sigma = 1.0$.

TIME

(b) $\beta_1 = 64^\circ$; $M_1 = 0.33$; $\sigma = 1.0$.

L-92408

Figure 22.- Rotating stall. 5,000 frames per second.

(c) $\beta_1 = 67^\circ$; $M_1 = 0.35$; $\sigma = 1.0$. L-92409

Figure 22.- Concluded.

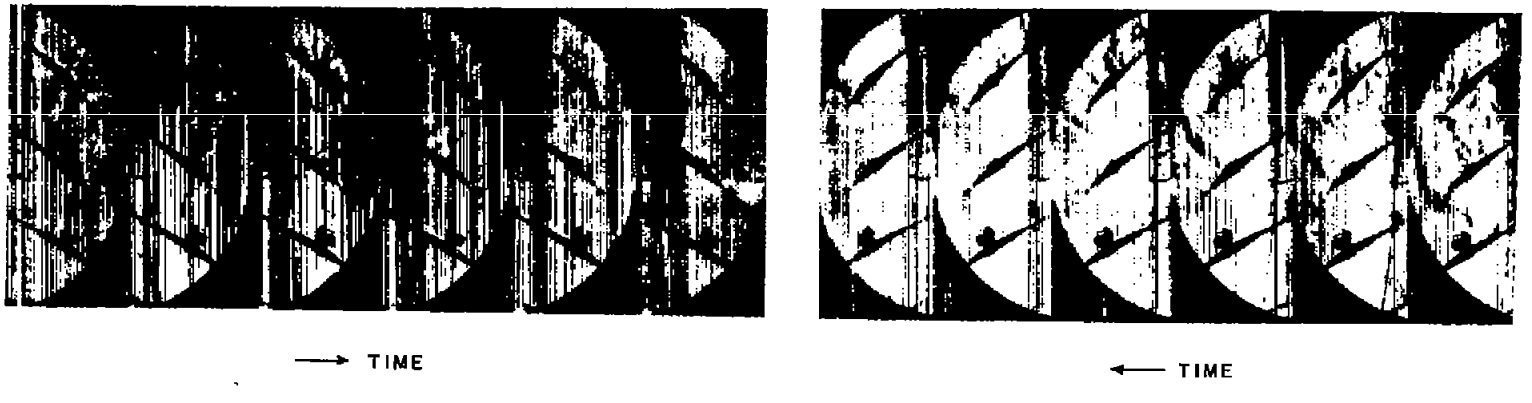

L-92410

Figure 23.- Vortex planes in cascade. 5,000 frames per second; $\beta_1 = 67^\circ$; $M_1 = 0.35$; $\sigma = 1.0$.

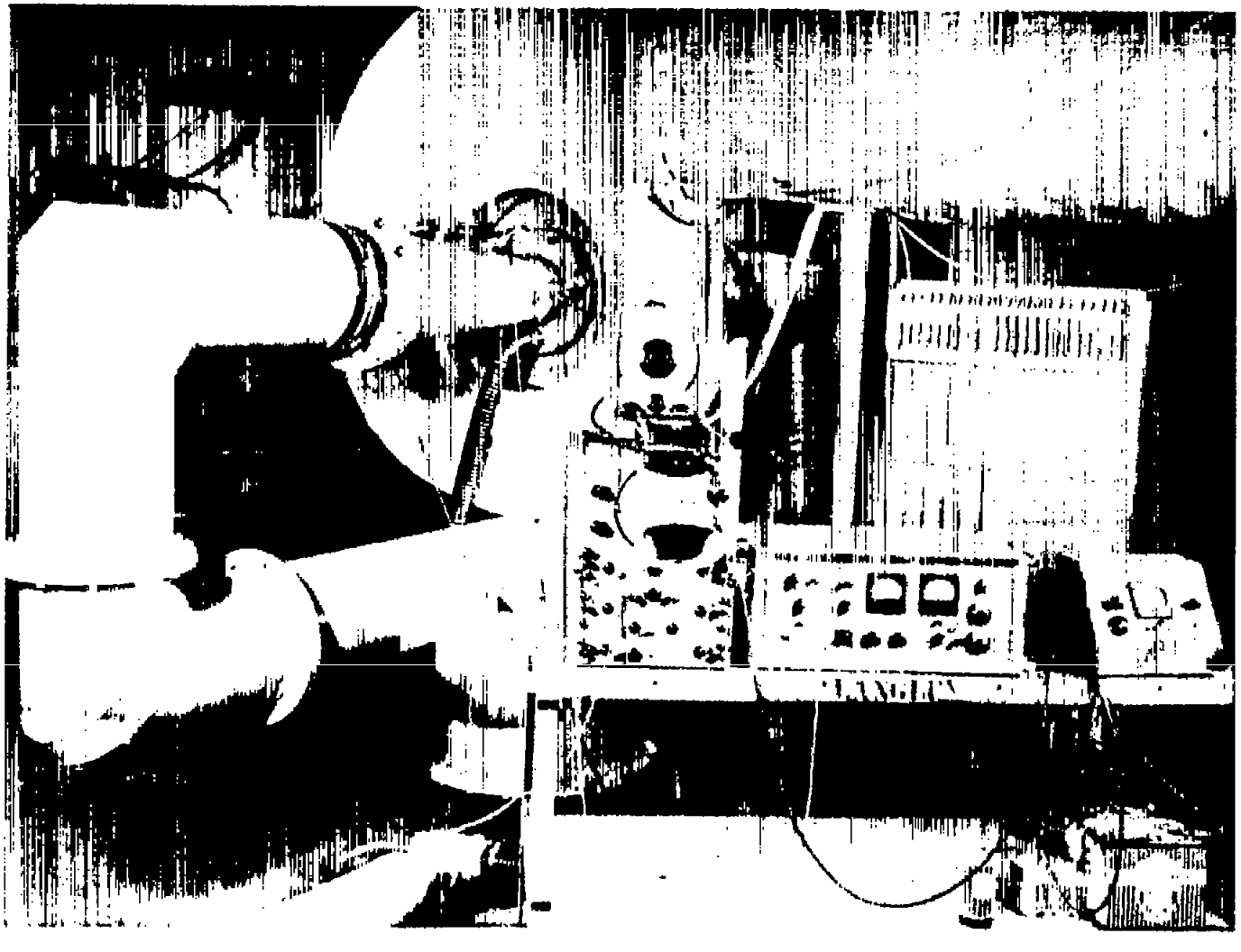

L-92411

Figure 24.- Hot-wire-anemometer equipment and cascade tunnel.

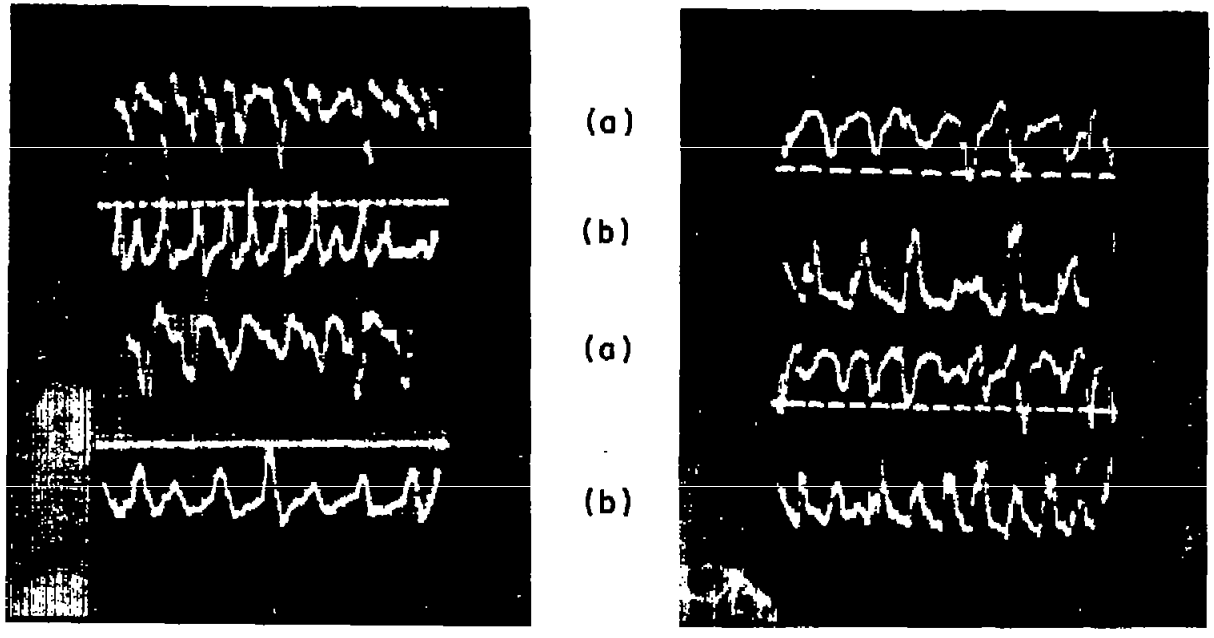

(a) $\beta_1 = 65.5^\circ$; $M_1 = 0.34$. (b) $\beta_1 = 68^\circ$; $M_1 = 0.35$.

Figure 25.- Hot-wire-anemometer traces from two probes upstream of cascade with probe (b) located nine blade spaces ahead of probe (a). Velocity increases toward center of oscillogram. Timing signals are for 500 cycles per second.

L-92412

Figure 26.- Rotating stall. 6,000 frames per second; $\beta_1 = 67°$; $M_1 = 0.65$; $\sigma = 1.0$.

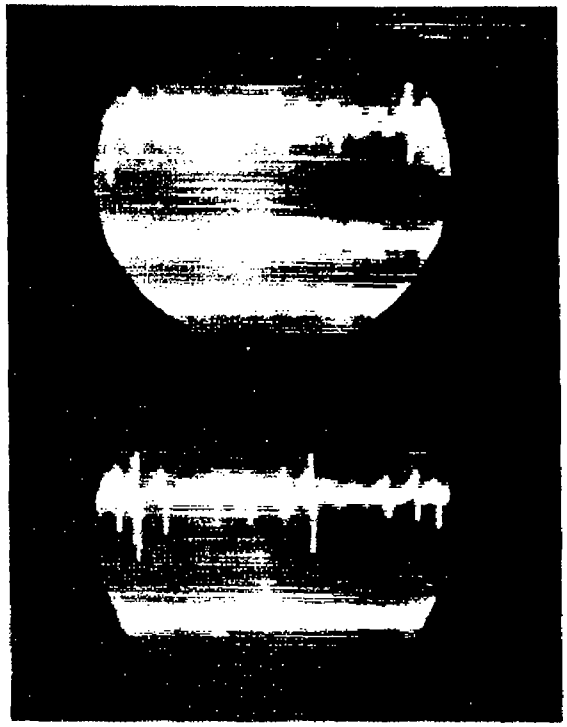

Figure 27.- Pressure fluctuations at tap (a) upstream and at tap (b) downstream of cascade. $\beta_1 = 68.5°$; $M_1 = 0.22$.

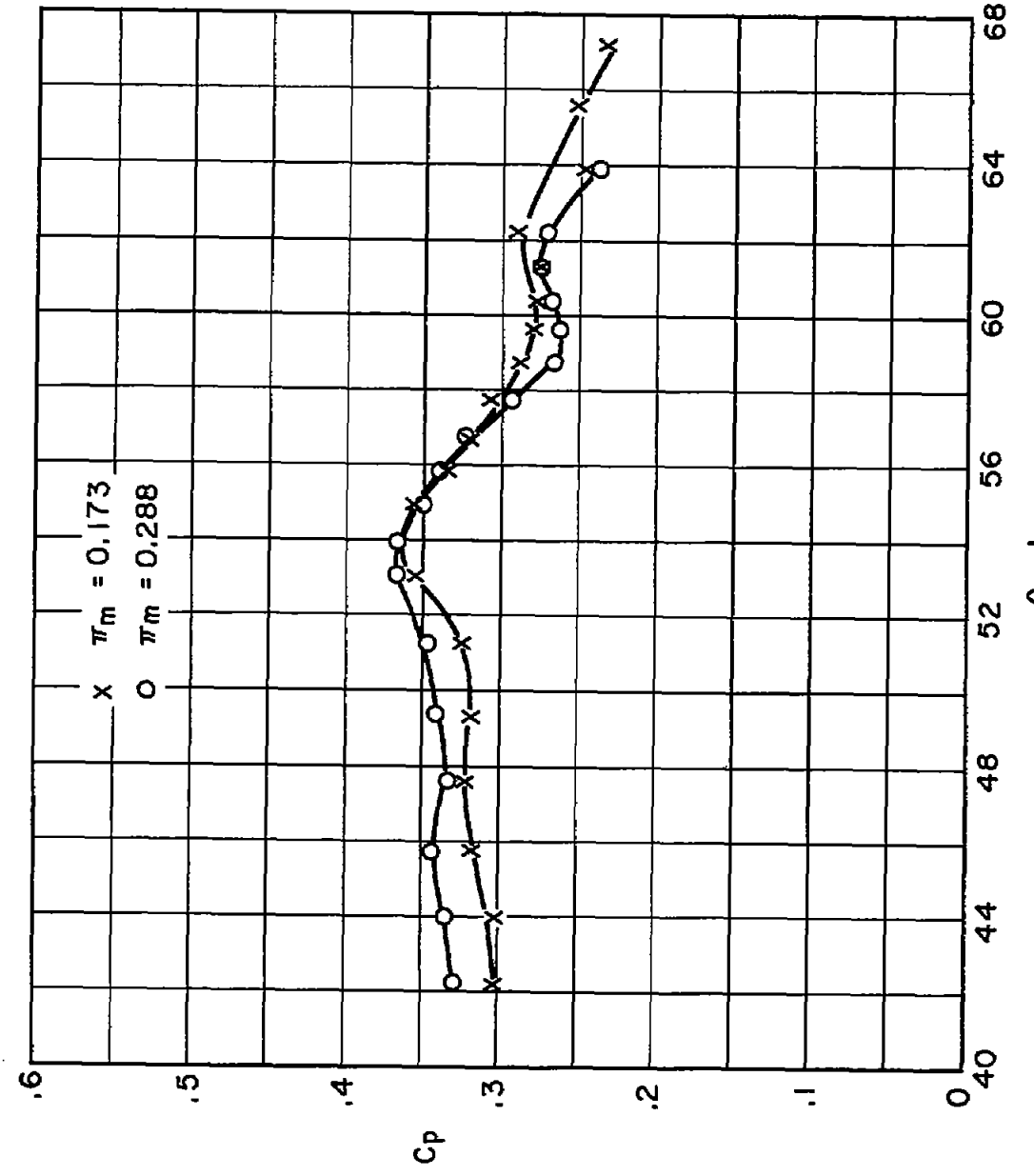

Figure 28.- Cascade pressure coefficient versus β_1 for $\sigma = 0.5$.

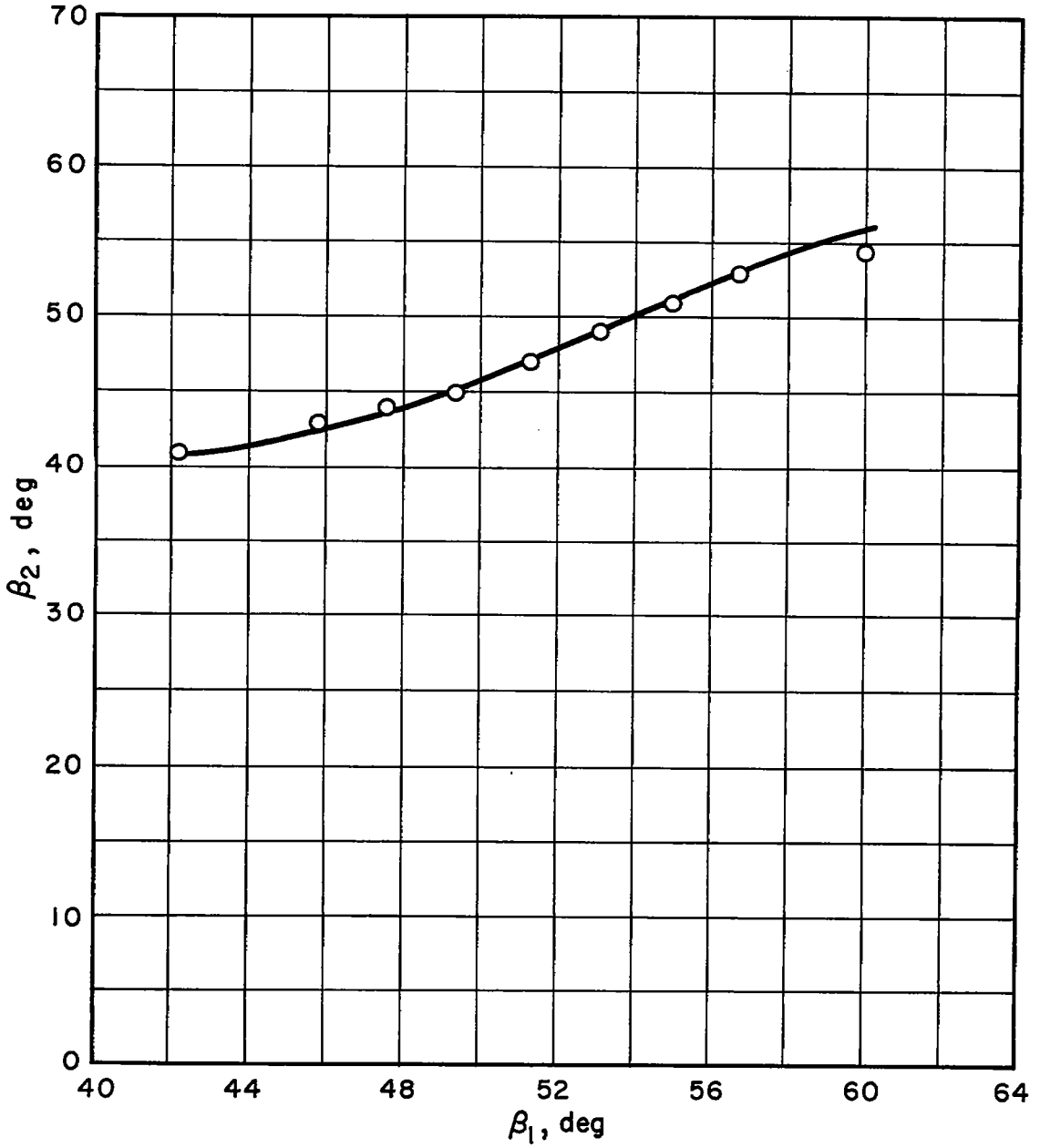

Figure 29.- Cascade performance. β_2 versus β_1 for $\sigma = 0.5$.

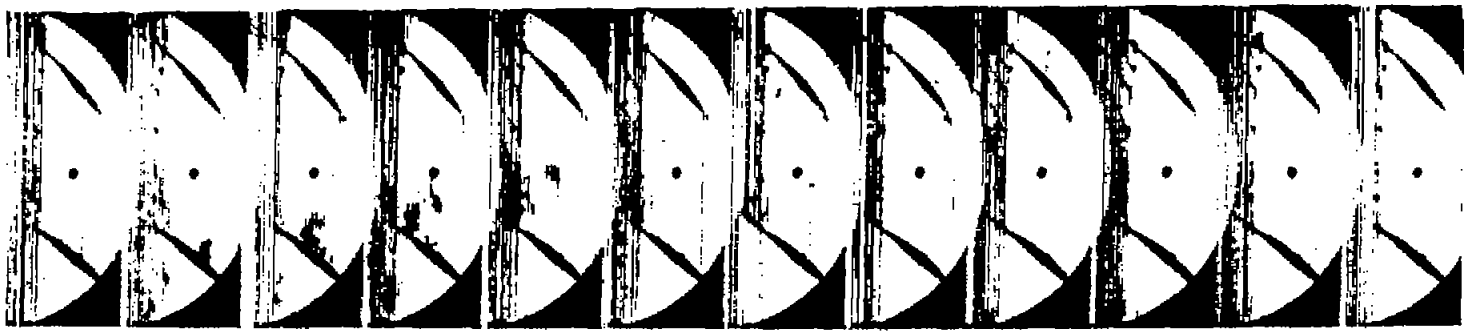

(a) $\beta_1 = 65^\circ$; $M_1 = 0.34$; $\sigma = 0.5$.

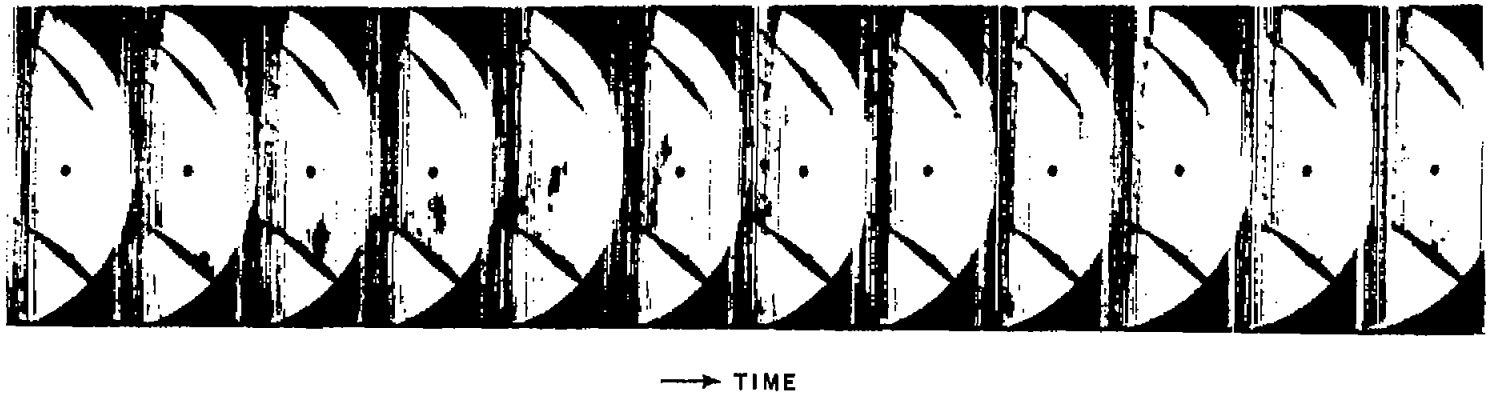

(b) $\beta_1 = 68.5^\circ$; $M_1 = 0.35$; $\sigma = 0.5$.

L-92413

Figure 30.- Rotating stall. 5,000 frames per second.

TIME ⟵

L-92414

Figure 31.- Rotating stall. $\beta_1 = 68.5^\circ$; $M_1 = 0.45$; 16-millimeter Fastax camera.

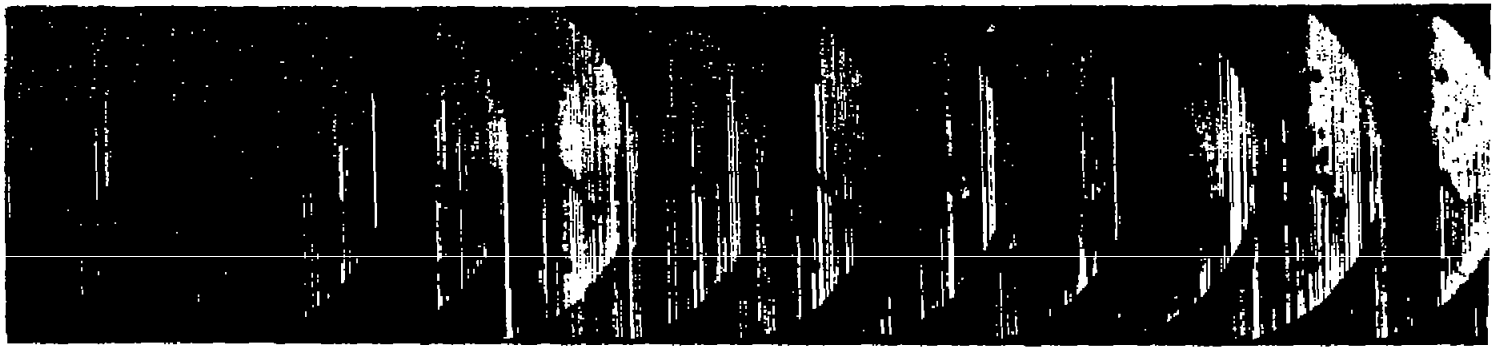

TIME ⟶

L-92415

Figure 32.- Rotating stall. 5,000 frames per second; $\beta_1 = 68.5^\circ$; $M_1 = 0.35$; $\sigma = 0.33$.

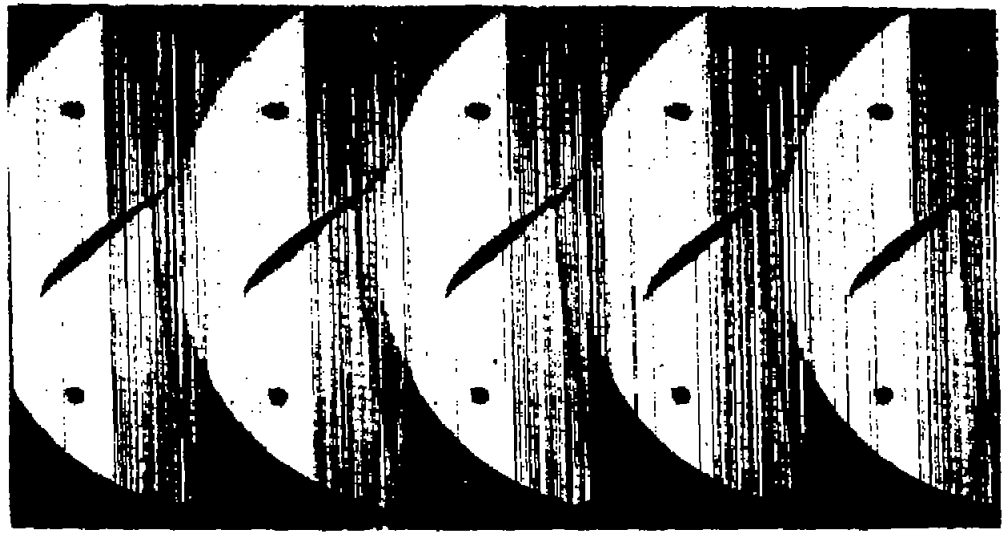

L-92416

Figure 33.- Stalled airfoil. 5,000 frames per second; $\beta_1 = 68.5°$; $M_1 = 0.35$; $\sigma = 0.16$.

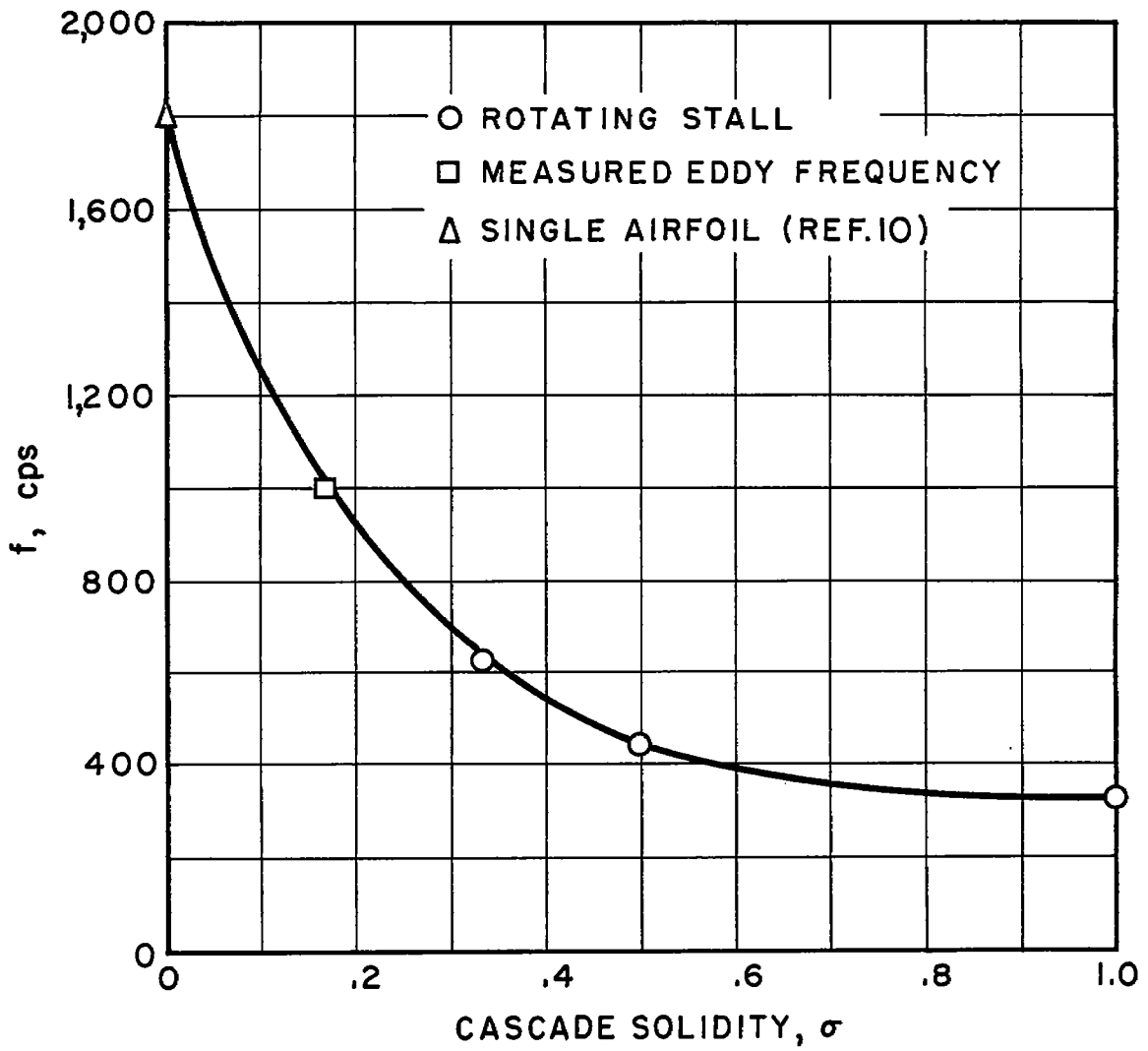

Figure 34.- Frequency of oscillations versus solidity. $\beta_1 = 68.5°$; $M_1 = 0.35$.

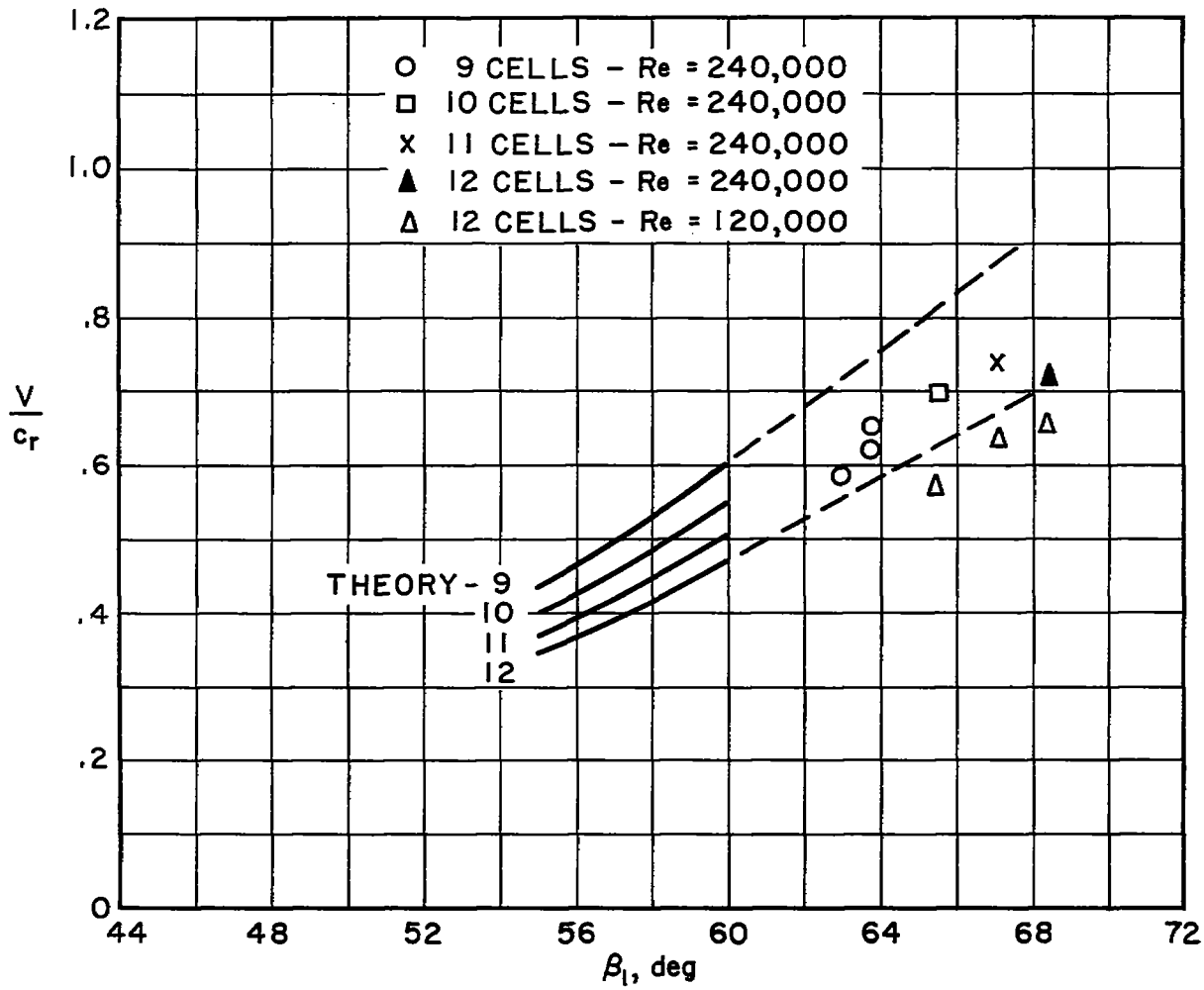

(a) $\sigma = 1.0$.

Figure 35.- Theoretical and experimental values of propagation velocity.

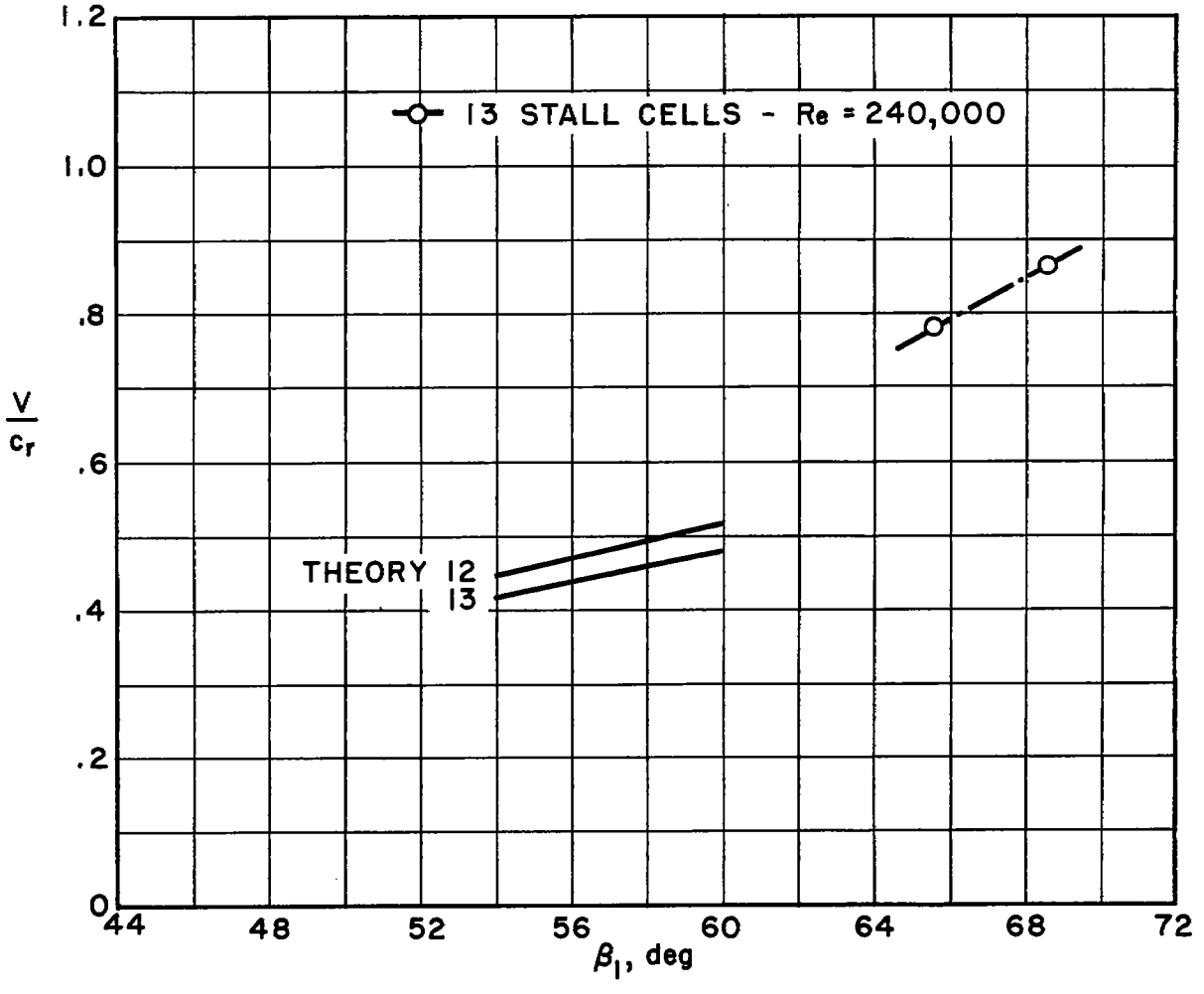

(b) $\sigma = 0.5$.

Figure 35.- Concluded.

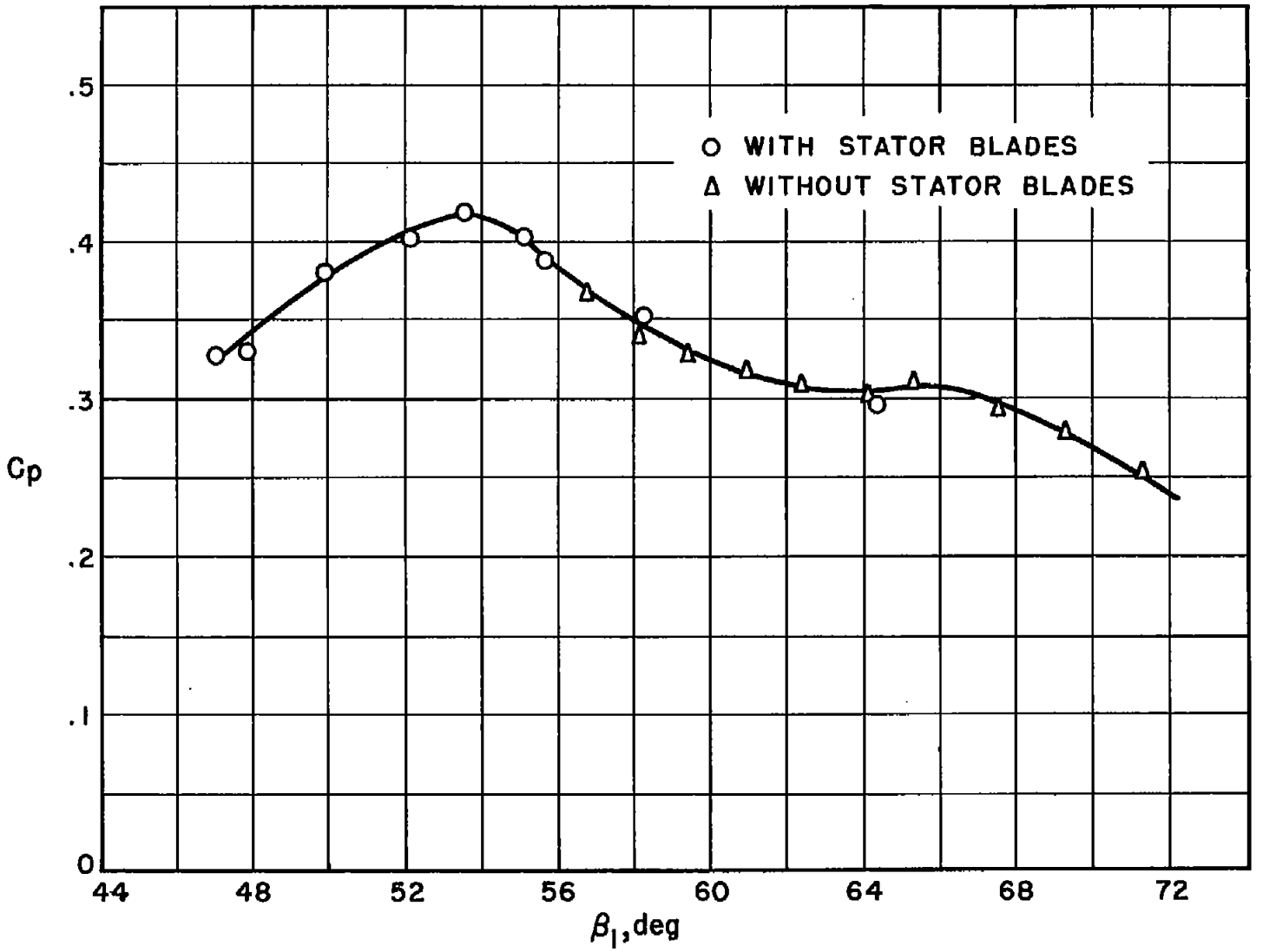

Figure 36.- Rotor performance. Pressure coefficient versus β_1.

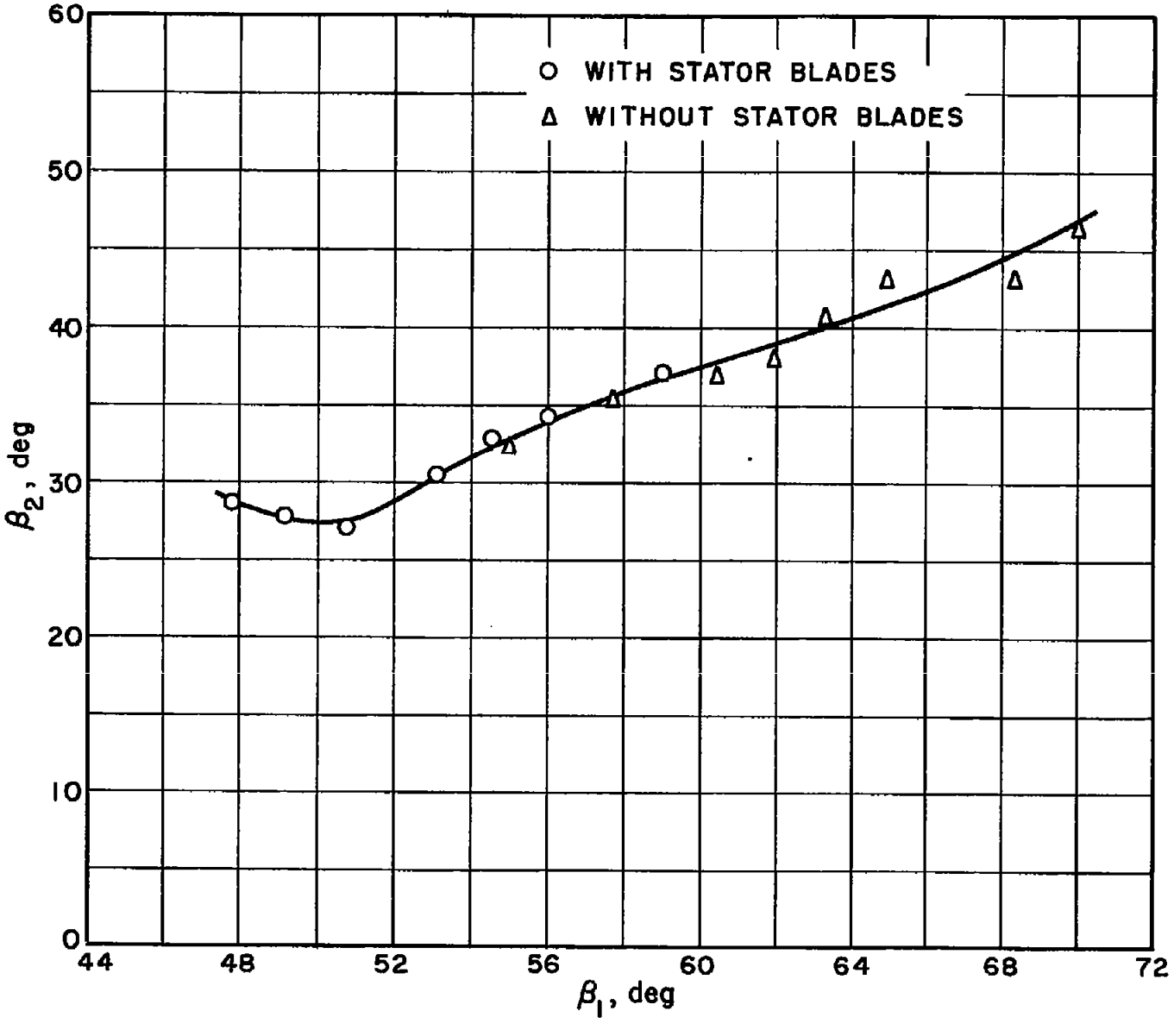

Figure 37.- Rotor performance. β_2 versus β_1.

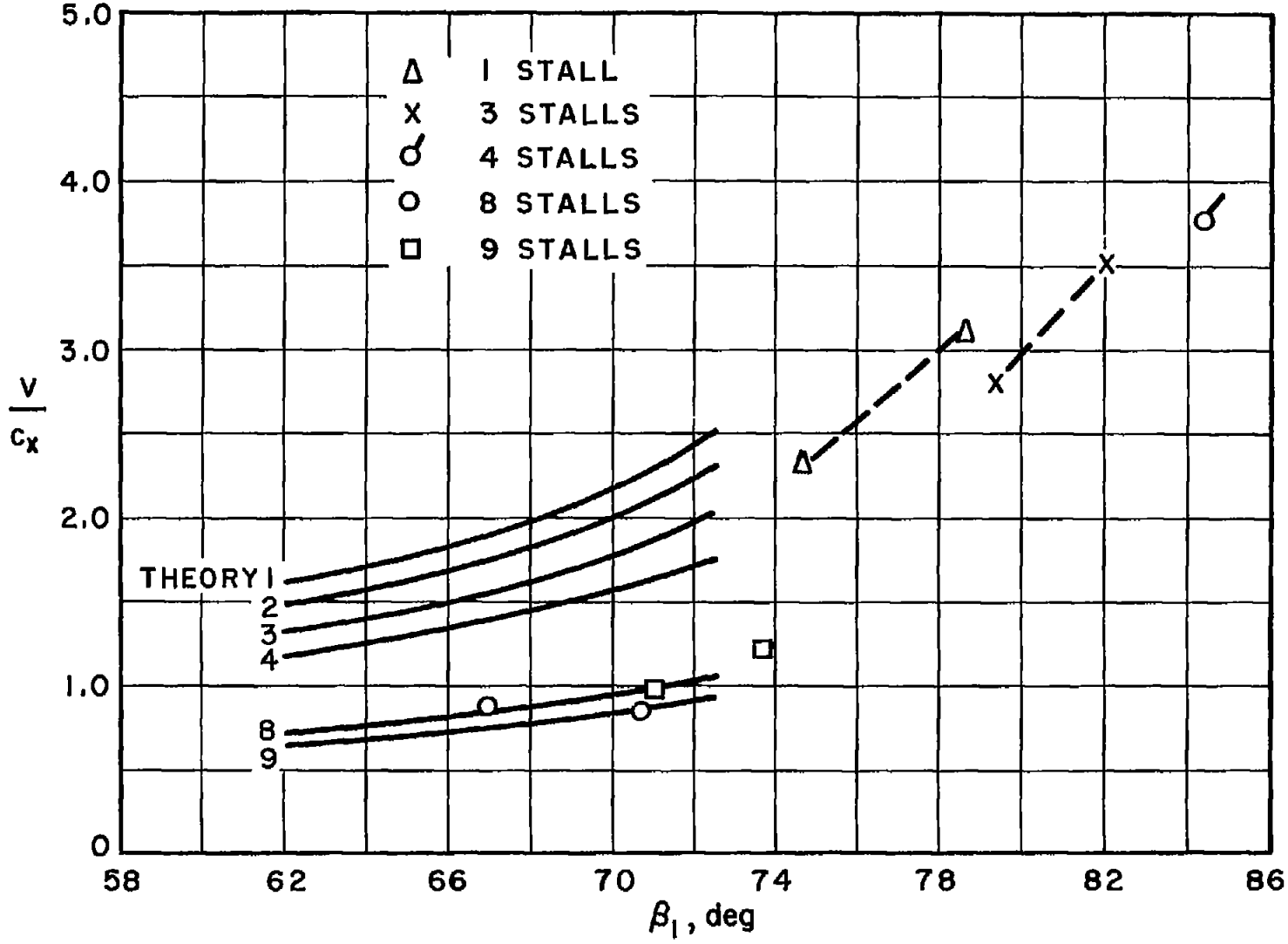

Figure 38.- Theoretical and experimental propagation velocities for rotor.